Pyrenoidal sequestration of cadmium impairs carbon dioxide fixation in a microalga

Florent Penen, M.-P. Isaure, Dirk Dobritzsch, Etienne Gontier, Hiram Castillo-Michel, Philippe Le Coustumer, Julien Malherbe, Dirk Schaumlöffel

Pyrenoidal sequestration of cadmium impairs carbon dioxide fixation in a microalga[#]

Florent Penen[1], Marie-Pierre Isaure[1], Dirk Dobritzsch[2], Hiram Castillo-Michel[3], Etienne Gontier[4], Philippe Le Coustumer[1,4,5], Julien Malherbe[1], Dirk Schaumlöffel[1*]

[1]CNRS / Université de Pau et des Pays de l'Adour / E2S UPPA, Institut des Sciences Analytiques et de Physico-Chimie pour l'Environnement et les Matériaux, UMR 5254, 64000 Pau, France

[2]Martin-Luther-Universität Halle-Wittenberg, Core Facility Proteomic Mass Spectrometry, Proteinzentrum Charles Tanford, Kurt-Mothes-Str. 3a, 06120 Halle (Saale), Germany

[3]ID21 Beamline, European Synchrotron Radiation Facility (ESRF), BP220, 38043 Grenoble, France

[4]Université de Bordeaux, Bordeaux Imaging Center UMS 3420 CNRS - US4 INSERM, Pôle d'imagerie électronique, 146 rue Léo Saignat, 33076 Bordeaux, France

[5]Université de Bordeaux, UF Sciences de la Terre et Environnement, Allée G. Saint-Hillaire, 33615 Pessac, France

[#]**Accepted manuscript :**
Penen, F., Isaure, M.-P., Dobritzsch, D., Castillo, H., Gontier, E., Le Coustumer, P., Malherbe, J., Schaumlöffel, D. (2020). Pyrenoidal sequestration of cadmium impairs carbon dioxide fixation in a microalga. *Plant, Cell & Environment*, **43,** 479-495
https://doi.org/10.1111/pce.13674

***Corresponding author:**

Dirk Schaumlöffel

CNRS / Université de Pau et des Pays de l'Adour / E2S UPPA, Institut des Sciences Analytiques et de Physico-Chimie pour l'Environnement et les, Matériaux, UMR 5254, 64000 Pau, France

Tel: (+33) 559 40 77 60

E-mail adress: dirk.schaumloeffel@univ-pau.fr

ABSTRACT

Mixotrophic micro-organisms are able to use organic as well as inorganic carbon sources and, thus, play an essential role in the biogeochemical carbon cycle. In aquatic ecosystems, the alteration of CO_2 fixation by toxic metals such as cadmium - classified as a priority pollutant - could contribute to the unbalance of the carbon cycle. In consequence, the investigation of cadmium impact on carbon assimilation in mixotrophic micro-organisms is of high interest. We exposed the mixotrophic microalga *Chlamydomonas reinhardtii* to cadmium in a growth medium containing both CO_2 and labeled ^{13}C-[1,2] acetate as carbon sources. We showed that the accumulation of cadmium in the pyrenoid, where it was predominantly bound to sulfur ligands, impaired CO_2 fixation to the benefit of acetate assimilation. TEM/X-EDS and µXRF/µXANES at Cd L_{III}-edge indicated the localization and the speciation of cadmium in the cellular structure. In addition, NanoSIMS analysis of the $^{13}C/^{12}C$ ratio in pyrenoid and starch granules revealed the origin of carbon sources. The fraction of carbon in starch originating from CO_2 decreased from 73% to 39% during cadmium stress. For the first time, the complementary use of high-resolution elemental and isotopic imaging techniques allowed relating the impact of cadmium at the subcellular level with carbon assimilation in a mixotrophic microalga.

KEYWORDS

Biogeochemical carbon cycle, CO_2 fixation, toxic metals, cadmium stress, subcellular imaging, NanoSIMS, synchrotron µXRF, µXANES, TEM/X-EDS, isotopic labeling, isotope ratio

INTRODUCTION

The increase of carbon dioxide concentration in the atmosphere over the past decades has been associated with global climate change. Therefore, investigation and understanding of the biogeochemical carbon cycle is of primordial importance. The terrestrial and oceanic biosphere plays a major role in the global carbon cycle by the production and conversion of organic matter (Field, Behrenfeld, Randerson & Falkowski, 1998). Plants have developed a process for CO_2 fixation into organic carbon using the enzyme ribulose-1,5-bisphosphate carboxylase/oxygenase (RuBisCO) which is regarded to be the most abundant protein in the biosphere (Ellis, 1979). Microalgae are small eukaryotic organisms where RuBisCO is concentrated in the specific organelle called the pyrenoid (Badger et al., 1998). Pyrenoid containing algae have been identified as being responsible for 28 - 44% of the global carbon fixation which underlines the key role of microalgae in the biogeochemical carbon cycle (Mackinder et al., 2016).

Eukaryotic algae are classically considered as photoautotrophic using light and inorganic compounds for energy and carbon fixation, or heterotrophic using only organic compounds. Recently, mixotrophy has been integrated into aquatic biogeochemical cycle modeling (Caron, 2016; Ward & Follows, 2016). Mixotrophic organisms are able to combine photoautotrophic growth conditions as well as heterotrophic nutrition. They are dominant among micro-algal communities in oligotrophic and eutrophic environments (Burkholder, Glibert & Skelton,

2008; Hartmann et al., 2012). To date, the consideration of mixotrophy in biogeochemical carbon cycle models is still at the beginning (Caron, 2016). Recently it has been shown that mixotrophy globally lead to an increase of the size of organisms in the aquatic food chain and thus enhances carbon sinking into the deep ocean by 35% (Ward & Follows, 2016).

Cadmium is a highly toxic metal and is considered as a priority pollutant in ecosystems (Campbell, 2006). In high polluted natural waters micromolar cadmium concentrations were found such as in the Tinto river in Spain (40 - 620 µM) (Aguilera & Amils, 2005) while for other natural waters lower Cd concentration are described, e.g. 2.4 - 17.8 nM in polluted Macedonian rivers (Ramani et al., 2014) and only 0.2 - 2 nM in a Swiss river (Xue & Sigg, 1998). Also, in polluted soils and soil solutions high cadmium concentrations were measured, for example, 5.4 - 45.5 µM Cd in soil solutions of soils close to a chemical engineering plant in Northern Taiwan (Lee, Lai & Chen, 2004) and 284 mg Cd per kg in paddy soils from Thailand (Simmons, Pongsakul, Saiyasitpanich & Klinphoklap, 2005). Moreover, Cd has been shown to be biomagnified in some aquatic food webs (Croteau, Luoma & Stewart, 2005; Ikemoto et al., 2008; Rouleau, Gobeil & Tjlve, 2006; Signa, Mazzola, Tramati & Vizzini, 2017). At the microbial level, this accumulation occurs in communities between bacteria and eukaryote organisms (Worden et al., 2015). In view of the importance of mixotrophy in the aquatic carbon cycle, the impact of toxic metals such as Cd on carbon assimilation in microalgae is of growing interest.

Chlamydomonas reinhardtii is a unicellular green alga which is found worldwide in soils and fresh water as its natural habitat. This alga is used as a model for many cellular processes (Dent, Han & Niyogi, 2001; Goto & Johnson, 1995; Harris, 1989; Merchant et al., 2006; Merchant, Kropat, Liu, Shaw & Warakanont, 2012; Merchant et al., 2007; Rochaix, M. Goldschmidt-Clermont & Merchant, 1998; Silflow & Lefebvre, 2001) including metallic stress (Hanikenne,

2003). Cadmium is known to inhibit its sexual reproduction (Goodenough et al., 1993), to limit photosynthesis activity (Faller, Kienzler & Krieger-Liszkay, 2005; Nagel & Voigt, 1989, 1995; Voigt & Nagel, 2002; Voigt, Nagel & Wrann, 1998) and to induce oxidative stress (Aksmann et al., 2014; Vega, Garbayo, Domínguez & Vigara, 2006). In order to reduce free intracellular Cd^{2+}, the microalga synthesizes thiol peptides such as phytochelatins (Bräutigam, Schaumlöffel, Preud'Homme, Thondorf & Wesenberg, 2011; Gekeler, Grill, Winnacker & Zenk, 1988) and sequesters Cd bound to polyphosphate granules into vacuoles which were compared to acidocalcisomes (Penen et al., 2017; Ruiz, Marchesini, Seufferheld, Govindjee & Docampo, 2001).

C. reinhardtii can grow photoautotrophically in the presence of light and CO_2, heterotrophically in the dark when acetate is available as an organic carbon source or mixotrophically with acetate, CO_2 and light (Johnson & Alric, 2013). In the latter case, CO_2 is photosynthetically fixed by RuBisCO (Johnson & Alric, 2012, 2013), while non-photosynthetic acetate assimilation begins by its incorporation into acetyl coenzyme A (acetylCoA) (Johnson & Alric, 2012, 2013). Then, acetylCoA is metabolized in the tricarboxylic acid (TCA) cycle in mitochondria or in the glyoxylate cycle in cytosol (Johnson & Alric, 2012, 2013; Singh, Shukla, Chary & Rao, 2014). Both acetate assimilation and photosynthesis lead to starch formation (Ball, Dirick, Decq, Martiat & Matagne, 1990; Heifetz, Förster, Osmond, Giles & Boynton, 2000; Johnson & Alric, 2012, 2013; Park et al., 2015). In spite of an abundant literature about carbon assimilation under mixotrophic conditions in *C. reinhardtii*, the impact of toxic metals on the carbon metabolism has not been investigated yet.

Ion beam and X-ray beam imaging techniques are powerful tools to study the isotopic and elemental composition of single-cells (Ortega, Devès & Carmona, 2009; Penen et al., 2016; Roschzttardtz et al., 2011; Sarret et al., 2013; Schaumlöffel et al., 2016). Nanoscale secondary

ion mass spectrometry (NanoSIMS) allows elemental and isotopic mapping with a resolution of about 50 nm. In biology, it is used to localize and to determine at a subcellular level the turnover of proteins and metabolites using stable isotopic tracers (^{13}C and ^{15}N) (Gao, Huang & Tao, 2016; Lechene et al., 2006). Moreover, when NanoSIMS is combined with transmission electron microscopy (TEM) in correlative imaging, isotopic tracers can be localized in the cell structure (Clode, Stern & Marshall, 2007; Hoppe, Cohen & Meibom, 2013; Kopp et al., 2015; Penen et al., 2016). NanoSIMS mapping has been also used to determine metal distributions in plants and microalgae (Hong-Hermesdorf et al., 2014; Moore et al., 2010, 2011, 2012). As complementary techniques, synchrotron micro X-ray fluorescence (µXRF) and micro X-ray absorption spectroscopy (µXAS) can be combined and directly applied on frozen hydrated samples to locate metals and decipher their structural environment, respectively, allowing the determination of metal distribution and speciation in subcellular regions of microalgae (Adams et al., 2016; Leonardo et al., 2014; Leonardo et al., 2016; Penen et al., 2017; Wang, Lv, Ma & Zhang, 2016).

Here, we investigated the impact of cadmium on carbon assimilation in *C. reinhardtii* grown under mixotrophic conditions. The objective was to relate subcellular cadmium localization and speciation with acetate and CO_2 assimilation. Microalgae were thus exposed up to 70 µM Cd and cultivated in the presence of labeled ^{13}C-[1,2] acetate to distinguish carbon originating from acetate assimilation or from photosynthesis. A multimodal approach at subcellular level allowed the localization of cadmium in the algal structure by TEM/X-EDS (X-ray energy dispersive spectroscopy) and the determination of carbon origins by measuring the $^{13}C/^{12}C$ ratio in the pyrenoid and starch using NanoSIMS. In addition, Cd was localized by µXRF, which was combined to µXANES (micro X-ray absorption near edge structure spectroscopy) at the Cd L_{III}-edge to identify Cd speciation. Our study showed that in *C. reinhardtii* cadmium sequestration in the pyrenoid impaired CO_2 fixation to the benefit of acetate assimilation.

MATERIALS AND METHODS

Biological material and growth conditions

Chlamydomonas reinhardtii wild type strain (SAG 11/32b, Experimental Phycology and Culture Collection of Algae at Goettingen University (EPSAG), Germany) was grown heterotrophically in a tris-acetate-phosphate medium (Harris, 1989) where ethylenediaminetetraacetic acid (EDTA) and $FeSO_4 \cdot 7H_2O$ were replaced by iron ethylenediamine-N,N'-bis(2-hydroxyphenylacetate) (Fe-EDDHA) to increase the availability of cadmium in solution. All chemicals and reagents were purchased from Sigma-Aldrich (Saint-Quentin Fallavier, France) unless stated otherwise. The composition of this TAP_{EDDHA} medium is described in Table S1. For carbon fixation experiments, the TAP_{EDDHA} (^{13}C) medium was prepared with ^{13}C-labeled acetate (sodium ^{13}C-[1,2] acetate, 99% ^{13}C, Sigma Aldrich) instead of acetic acid and pH was equilibrated to 7 with a HCl solution. Microalgae grew at 22 °C under constant illumination (by one Osram 827 and two Osram 840 fluorescent tubes) and constant agitation (120 rpm). Fresh medium was inoculated with stock culture at the end of exponential phase to reach an initial optical density at 730 nm (OD_{730nm}) of 0.040. Micro-algae were exposed to 10, 20, 30, 40, 50 and 70 µM of $CdCl_2$ added 24 h after the inoculation while control cultures were grown in parallel without Cd exposure (control). For controls and each Cd concentration three independent algal cultures were grown (triplicates) and used for replicated determination of the growth rate, chlorophyll and starch concentrations, and cadmium uptake.

As the main aim of this study was the investigation of the cadmium stress response at cellular level during the exponential growth phase, cells were exposed to Cd after 24h. Therefore changes in the lag phase, the delay before the start of exponential growth, were not assayed since this delay allowed the adaptation required for cells to begin the experience of new

environmental conditions, i.e. cadmium exposure in this study. The cell cycle of *C. reinhardtii* is about 24 h which is confirmed with the start of the exponential phase at this time point. This means that under these conditions the cells of the second (and third) cell cycle are exposed. Cells were harvested after 72 h for different analyses, i.e. at the end of the third cell cycle when these cells experienced similar exposure conditions. It is a good approximation although cultivation was not synchronized. This procedure also applied in our previous studies (Bräutigam, Schaumlöffel, Preud'Homme, Thondorf, & Wesenberg, 2011; Bräutigam, Schaumlöffel, Krauss, & Wesenberg, 2009; Penen et al., 2017).

The concentrations of free metals in the medium were simulated (Table 1) with the freeware Visual MINTEQ 3.0 (vminteq.lwr.kth.se/visual-minteq-ver-3-0/) (Gustafsson, 2013) using Lindsay's database containing thermodynamic equilibrium constants compiled by Lindsay (1979). Before use, glassware was washed with 5% HNO_3. All solutions were prepared with ultrapure water (18 MΩ cm at 25 °C) obtained from a Milli- Q system (Millipore, Bedford, MA).

Growth rate determination

Optical density at 730 nm (OD_{730nm}) was measured every 12 h in each control and Cd-exposed algal cultures, grown in triplicate, using a spectrophotometer. Growth rates μ were calculated as follows: $\mu = (\ln N_f - \ln N_i)/\Delta t$. N_f was the OD_{730nm} of the culture measured at the end of the exponential phase. N_i was the OD_{730nm} of the culture at the beginning of the exponential phase and Δt was the duration of the exponential phase (in days). Relative growth rate was expressed as the ratio μ/μ_0 determined during the exponential phase of growth (μ: growth rate during cadmium exposure, μ_0: growth rate in control conditions). The Excel macro REGTOX (http://www.normalesup.org/~vindimian/en_index.html) was used to calculate the half maximal efficient concentrations (EC_{50}) applying the Hill model.

196 **Chlorophyll concentration measurement**

197 The chlorophyll concentration assay was adapted from Arnon *et al.* (Arnon, 1949). After 72 h
198 cultivation, 1 ml of each control and Cd-exposed algal cultures (grown in triplicate) was
199 centrifuged at 13000 × g for 1 min. Each algal pellet was resuspended in 1 mL of 80% acetone
200 and vortexed for 2 min. Then, solubilized chlorophyll was separated from cell debris by a
201 centrifugation at 13000 × g for 4 min. After that, the concentration (C) of chlorophyll a and b
202 in the culture medium was determined spectrophotometrically at 652 nm and calculated as
203 follows: $C = Abs_{652nm} \times 1000 / 34.5$ with C in mg mL^{-1}. Finally, in order to relate the chlorophyll
204 content to the biomass, the determined chlorophyll concentration was normalized to the optical
205 density at 730 nm whose value is proportional to the number of cells in the medium (unit: µg
206 mL^{-1} OD_{730nm}^{-1}).

207 **Starch concentration measurement**

208 After 72 h cultivation, microalgae were harvested from in triplicate grown control and Cd-
209 exposed (70 µM) algal cultures by centrifugation at 3000 × g for 3 min and each pellet was
210 resuspended in 1.5 mL water. In order to estimate the dry biomass, a 0.5 mL aliquot from each
211 sample was dried at 60 °C for 24 h and the resulting pellet was weighted. The remaining 1 mL
212 samples were washed once with water and once with 80% ethanol, and centrifuged (3000 × g
213 for 3 min). Then, each pellet was boiled in 2 mL water for 10 min. Finally, starch concentrations
214 were determined in these extracts, using the enzymatic starch assay kit HK (Sigma Aldrich)
215 described in Delrue *et al.* (1992).

216 **Cadmium uptake**

217 After 48 h cadmium exposure (70 µM), microalgae were harvested from in triplicate grown
218 cultures by centrifugation at 3000 × g for 3 min. In order to obtain the intracellular Cd

concentration, each algal pellet was subjected to the following washing protocol according to Macfie *et al.* (1994): a first time in water, then twice in a mix of Na_2-EDTA (1 mM) / $CaCl_2$ (3.77 mM) and finally in water with centrifugation between in (3000 × g for 3 min). The remaining pellets were dried at 60°C for 24 h and weighted. This dry algal biomass was digested in a mixture of 1 mL 70% (v/v) HNO_3 and 1 mL 30% (v/v) H_2O_2 at 80 °C for 3 h. Samples were then diluted to reach a 2% HNO_3 concentration. The cadmium concentration was determined by ICP-MS (Inductively Coupled Plasma Mass Spectrometry, 7500 model, Agilent Technologies).

Sample preparation for TEM/X-EDS and NanoSIMS

Microalgae from a control and a Cd-exposed (70 µM) culture containing ^{13}C-labeled acetate in the medium were harvested after 72 h of inoculation by centrifugation at 3,000 × g for 3 min. A protocol including high pressure freezing, and freeze substitution followed by resin inclusion was used to preserve cell integrity. For high-pressure freezing, each microalgae pellet was resuspended and incubated for 1 h in 150 mM mannitol. After a centrifugation at 3000 × g for 3 min, the harvested cells were included in agarose 2%. Then, the inclusion was plunged in cryo-protectant 1-hexadecene and high-pressure freezing was performed immediately (EM HPM 100, Leica Microsystems, Vienna, Austria). Samples were maintained in liquid nitrogen until the freeze-substitution steps.

Freeze-substitution was adapted from O'Toole's protocol (O'Toole, 2010). Under liquid nitrogen, algal samples were post-fixed in 1% osmium tetroxide, 0.1% uranyl acetate and 0.25% glutaraldehyde in anhydrous acetone and transferred into the Automatic Freeze Substitution System AFS2 (Leica microsystems). Temperature was maintained at -90 °C for 3

d and then warmed to -30 °C for 8 h. Samples were removed from freeze-substitution system, kept at 0 °C for 1 h and washed with water-free acetone.

Resin inclusion was carried out at room temperature. Samples were embedded in epoxy resin (EPON 812, Delta Microscopies, Mauressac, France) using a graded resin and acetone series. The following steps were applied for infiltration: 3:1 acetone:resin, 1:1 acetone:resin, 1:3 acetone:resin, and 2 baths with 100% resin. Finally, resin embedded samples were polymerized for 48 h at 60 °C.

Samples were cut in 70 nm and 300 nm sections for TEM and NanoSIMS, respectively, using a diamond knife (Diatome, Biel-Bienne, Switzerland) on an ultra-microtome [EM Ultracut-UC7, Leica Microsystems) and placed on the respective sample holder. In order to carry out correlative imaging by TEM and NanoSIMS, a first 70 nm section was placed on a copper grid for TEM and then, an adjacent 300 nm section was placed on a silicon wafer (Wafer Solution, Le Bourget du lac, France) for NanoSIMS as previously described (Penen et al., 2016). Cells were localized and observed first by TEM and then, relocalized and analyzed by NanoSIMS.

TEM/X-EDS analysis

A transmission electron microscope FEI TECNAI 12 (Eindhoven, The Netherlands) using an accelerating voltage 120 kV and equipped with an X-Energy Dispersive Spectroscopy (X-Flash 6T 60 BRUKER-SYNERGIE 4, Evry, France) was used. The parallel electron beam of the nanoprobe was focused on 0.25-1.2 µm areas. Under these conditions X-EDS spectra of 1-2k counts s^{-1}, a deadtime of 15-20% and analytical time of 120 - 240 s per spectrum were generated.

NanoSIMS analysis

A nanoscale secondary ion mass spectrometer NanoSIMS 50L (CAMECA, Gennevilliers, France) was used to perform SIMS analysis. This device was equipped with a primary Cs^+ ion source (lateral resolution down to 50 nm) for the mapping of electronegative elements, and with a novel O^- RF plasma primary ion source enabling a high sensitivity for electropositive elements combined to a high lateral resolution (40 nm lateral resolution) (Malherbe et al., 2016). The seven parallel electron multiplier detectors equipped on the NanoSIMS 50L instrument allowed detection of seven elements at the same time. In order to remove major interferences on the chosen element masses, the mass resolution (M/ΔM) was tuned to be about 5000. Initially, ion maps (256×256 pixels, 64-144 µm²) of $^{12}C^-$, $^{13}C^-$, $^{12}C^{14}N^-$ (for N detection) and $^{32}S^-$ were carried out using the primary Cs^+ ion source. Mapping of $^{31}P^+$ and $^{40}Ca^+$ was then performed using the O^- RF plasma primary ion source.

NanoSIMS data processing

Image processing was performed using ImageJ software (v.1.48, Wayne Rasband, National Institutes of Health (NIH), Bethesda, MD, USA). Processing of NanoSIMS images required additionally the openMIMS plugin developed at the National Resource for Imaging Mass Spectrometry (NRIMS, Cambridge, MA, USA). Ion maps were corrected for detector dead time (44 ns) with the openMIMS plugin and the $^{13}C/^{12}C$ ratio maps were corrected for the mass bias as a function of the $^{13}C/^{12}C$ ratio measured on microalgae not enriched in ^{13}C. The $^{13}C/^{12}C$ ratio was measured in regions of interest (ROI) defined on pyrenoid and starch granules of six control cells and six Cd-exposed cells as detailed in Figure S1. The isotopic enrichment of ^{13}C was expressed as its relative abundance $\delta^{13}C$ compared to the ^{13}C natural isotopic abundance and calculated using the following formula:

$$\delta^{13}C = \frac{R_{sample}}{R_{nat}} - 1 \quad (1)$$

where R_{sample} is the measured $^{13}C/^{12}C$ ratio in the ROI of the cells and R_{nat} is the natural carbon isotope ratio.

The origin of carbon in starch granules from either acetate or CO_2 as carbon source was determined by data processing adapted from Terrado et al. (2017). First, the fractional abundance F_{starch} of the carbon isotope ^{13}C in starch granules of the sum of both carbon isotopes is given as (in percentage):

$$F_{starch} = \frac{^{13}C}{^{13}C + ^{12}C} \times 100 \quad (2)$$

which can also be expressed as

$$F_{starch} = \frac{R_{starch}}{1 + R_{starch}} \times 100 \quad (3)$$

where R_{starch} is the $^{13}C/^{12}C$ ratio measured in the ROI within starch granules. Then, the origin of starch carbon was determined using the following formulas:

$$F_{starch} = F_{acetate} \times f_{acetate} + F_{CO2} \times f_{CO2} \quad (4)$$

$$\text{with:} \quad f_{acetate} + f_{CO2} = 1 \quad (5)$$

$$f_{acetate} = \frac{F_{starch} - F_{CO2}}{F_{acetate} - F_{CO2}} \times 100 \quad \text{and} \quad f_{CO2} = \frac{F_{starch} - F_{acetate}}{F_{CO2} - F_{acetate}} \times 100 \quad (6)$$

The formula (6) results from (4) and (5) where $F_{acetate}$ and F_{CO2} are the fractional abundance of ^{13}C in the carbon sources acetate (99%) and CO_2 (1.09%), respectively, and $f_{acetate}$ and f_{CO2} represent the percentage of the origin of carbon within the ROI (starch granule) from the respective source.

Samples preparation for synchrotron-based techniques

306 Microalgae from a control and a Cd-exposed (70 µM) culture were harvested after 72 h of
307 inoculation by centrifugation at 3000 × g for 3 min. They were rapidly washed in ultrapure
308 water three times to remove metals and organic compounds weakly adsorbed on the cell wall.
309 Two sample preparations were used.

310 For µXRF and Cd L_{III}-edge µXANES, droplets of microalgae suspension were deposited on 4
311 µm-thick Ultralene film (SPEX sample prep Metuche, NJ). After decantation for 10 min,
312 microalgae were frozen into liquid nitrogen-chilled isopentane (-160 °C).

313 For Cd L_{III}-edge XANES bulk analysis, the algae pellet was frozen in liquid nitrogen,
314 homogenized and pressed as a 5 mm frozen pellet. All the samples were kept frozen at -80 °C
315 until measurements and transferred to the sample stage in their hydrated frozen state.

316

317 **µXRF imaging**

318 Measurements were performed on the ID21 beamline at the European Synchrotron Radiation
319 Facility (ESRF, Grenoble, France) equipped with a fixed exit Si(111) two-crystal
320 monochromator (Cotte et al., 2017). The X-ray photons were focused by a KB mirror system
321 providing a sub-micron resolution of 0.6 µm (H) × 0.3 µm (V) FWHM on the sample. The X-
322 ray fluorescence signal was recorded with a large 100 mm^2 SDD detector (Bruker) while the
323 samples were scanned to obtain elemental maps. All the measurements were carried out under
324 cryogenic conditions at -160 °C using a liquid N_2 cryostat to limit beam radiation damage. The
325 fluorescence signal was normalized by the incident photon intensity (I_0) measured with a
326 photodiode. Phosphorus, sulfur, chloride, and cadmium maps were recorded using an incident
327 energy of 3570 eV, below the absorption edge of potassium, while potassium and calcium maps
328 were recorded at 4100 eV as described in Isaure *et al.* (2006). The fluorescence signal was

deconvoluted from fluorescence background and fluorescence elemental overlapping to obtain elemental maps using the PYMCA software (Solé, Papillon, Cotte, Walter & Susini, 2007).

Cd L_{III}-edge µXANES and XANES. µXANES spectra were recorded with the same lateral resolution as for µXRF in fluorescence mode on points of interest visualized on the µXRF maps. For Cd model compounds and bulk samples, XANES spectra were recorded in fluorescence mode with a defocused beam (100 µm × 100 µm). Measurements were also done under cryogenic conditions to limit radiation damage and speciation change. µXANES and XANES spectra were collected in the energy range 3520-3590 eV. Approximately 30 scans were calibrated with a metallic Cd foil, averaged, and normalized according to standard methods using ATHENA software (Ravel & Newville, 2005). Then, experimental normalized spectra were compared to a library of standard spectra previously collected (Huguet et al., 2012; Isaure et al., 2006, 2015; Penen et al., 2017). A fingerprint approach was used to simulate the unknown spectra by linear combination fits (LCFs) of Cd model compounds as described by Isaure *et al.* (2006). The quality of the fits was estimated by the normalized sum-squares residuals $NSS = \Sigma(Xanes_{experimental} - Xanes_{fit})^2/\Sigma(Xanes_{experimental})^2 \times 100$, in the 3520-3580 for µXANES spectra and 3520-3590 eV range for XANES spectra. Linear combination fits with one, two and three components were tested and the combination with n+1 components was retained if the NSS parameter decreased more that 20% in comparison to the fit with n components (Figure S2). The uncertainty of the proportion of each compound was estimated to 10% (Isaure et al., 2015).

Statistics

One-way ANOVA followed by a post-hoc Tuckey test Statistical analyses were performed on growth rate, chlorophyll concentration, starch concentration and $^{13}C/^{12}C$ ratio measured on NanoSIMS maps to identify significant differences among the different conditions. Results

were considered significant for a $p < 0.05$. Kruskal-Wallis one-way analysis of variance on ranks ($p<0.05$) was performed when the condition of homogeneity of variances was not respected.

RESULTS

Availability of cadmium and essential trace elements in TAP_{EDDHA} medium

In a first approach, cadmium availability in TAP_{EDDHA} medium, i.e. free Cd^{2+} concentration, was simulated using Visual Minteq software (Table 1). Concentrations of 10, 20, 30, 40, 50 and 70 µM of $CdCl_2$ added to the medium correspond to free ionic Cd concentrations of 1, 4, 7, 10, 13 and 20 µM. Cd availability was thus increased by 10 compared to the classic TAP medium for the higher Cd concentration.

The free ion concentrations of several essential trace elements in the TAP_{EDDHA} medium were markedly different from that in the original TAP medium (Table 1). Most important, the concentration of free Zn^{2+} increased by 10000 and of free Cu^{2+} by 100 whereas Co^{2+} availability decreased by 10000 compared to the classic TAP medium.

Cadmium exposure leads to starch accumulation

C. reinhardtii was exposed to a range of 10-70 µM $CdCl_2$ for 48 h in TAP_{EDDHA} medium and relative growth rates were measured in order to determine Cd efficient concentrations (EC_x) with the Hill model (Figure 1A). Up to 20 µM Cd, no significant effect on the algae growth was observed (EC_5 = 22 µM Cd [15–31 µM Cd $CI_{95\%}$]) but increasing Cd concentrations induced a strong decrease of the relative growth rate (EC_{50} = 74 µM Cd [67–86 µM Cd $CI_{95\%}$]). In order to investigate the impact of cadmium on *C. reinhardtii* in stress conditions, the Cd exposure concentration of 70 µM (i.e. 20 µM free Cd^{2+}) was applied in this study since it was the nearest to EC_{50} value. These concentrations can seem quite high compared to other studies

376 focused on Cd concentrations in the 10-100 nM range (Stoiber et al. 2012, Lavoie et al. 2012)
377 . However, contrary to these studies, the present experiments were carried out in mixotrophic
378 conditions, which likely modified the cell response. Our observations support that under
379 mixotrophic conditions *C. reinhardtii* was more resistant against Cd stress.

380 When exposed to 70 µM Cd, the intracellular cadmium concentration was 1530 ± 132 µg g^{-1}
381 (dry weight). The global impact of this cadmium stress on *C. reinhardtii* vitality was examined
382 by the determination of growth rate, chlorophyll concentration and starch concentration (Figure
383 1B, C and D). Compared to the control condition, Cd induced a decrease of the growth rate
384 (from 0.76 ± 0.05 to 0.39 ± 0.06 d^{-1}) and the chlorophyll concentration (from 8.3 ± 0.4 to 6.4
385 ± 0.3 µg mL^{-1} OD_{730nm}^{-1}) while starch concentration was increased (from 47.6 ± 4.7 to 87.9 ±
386 13.2 mg g^{-1}). These results showed an important stress in *C. reinhardtii* when it exposed to 70
387 µM Cd leading to an impaired photosynthesis and an accumulation of starch. Carbon
388 metabolism in *C. reinhardtii* was thus strongly impacted by Cd toxicity.

389 **Cadmium sequestration in pyrenoid and vacuoles**

390 *C. reinhardtii* cells exposed to 70 µM Cd for 48 h were examined by TEM/X-EDS and
391 NanoSIMS (Figure 2). Figure 2 A and B show that cell structure was altered by Cd exposure,
392 particularly the chloroplast where the pyrenoid and its starch shell were destructured. The
393 starch plaques were also more abundant in the Cd-exposed cells corroborating the increase of
394 starch measured by enzymatic digestion.

395 Elemental composition of organelles observed on TEM micrographs (Figure 2C, F) was
396 determined on their corresponding NanoSIMS elemental maps (Figure 2E, H). Vacuoles were
397 rich in calcium, phosphorus and sulfur. Pyrenoids were characterized by a composition rich in
398 sulfur and nitrogen, which could be attributed to the high concentration in proteins (RuBisCO
399 in particular) inside this organelle. Moreover, pyrenoids were surrounded by a halo of

phosphorus which did not necessarily correspond to the starch shell. Finally, starch shells and starch plates were rich in nitrogen.

Additional X-EDS analysis (Figure 2D, G) revealed that cadmium concentration was high in the pyrenoid. This pyrenoidal sequestration of Cd could thus be responsible for Cd toxicity in *C. reinhardtii*. Furthermore, Cd was localized beside Ca and P in electron dense bodies in vacuoles suggesting a cadmium sequestration in calcium polyphosphate granules as confirmed in our previous study by µXANES analysis (Penen et al., 2017). It is important to note that the elemental composition of vacuoles and pyrenoid determined by NanoSIMS was confirmed by the X-EDS measurements.

Cadmium localized in pyrenoid is preferentially bound to sulfur ligands

Elemental µXRF maps (Figure 3A) of *C. reinhardtii* cells exposed to 70 µM Cd for 48 h corroborated the elemental distribution obtained by TEM/X-EDS and NanoSIMS analysis (Figure 3A). A sulfur spot was present in each cell which corresponded to the pyrenoid. Although cadmium was detected at low level in the whole cells, it was highly concentrated in one spot in each cell co-localized with sulfur, confirming its pyrenoidal sequestration. In addition, phosphorus, calcium, and to a lesser extent cadmium were co-localized in spots of 1 µm size representing Ca polyphosphate granules in vacuoles.

In combination with µXRF, µXANES gave information about Cd binding ligands in areas of interest evidenced by µXRF. In contrast, XANES collected in bulk samples allowed to determine the average *in situ* cadmium binding in the microalgae. Cd L_{III}-edge XANES was demonstrated powerful to distinguish sulfur from oxygen ligands due to absence of a peak at 3539 eV in sulfur binding atoms (Isaure et al., 2006). Moreover, as indicated by arrows in Cd reference XANES spectra in figures 3B and 3C, the second oscillation was shifted to higher energy values for Cd-acetate and Cd-malate where Cd is bound to carboxyl groups compared

to Cd bound to phosphate groups in Cd-phosphate and Cd-phytate (Penen et al., 2017). This enabled a differentiation between the oxygen donor ligands in Cd-carboxyl and Cd-phosphate. In contrast, Cd-phytochelatin 2 (Cd-PC_2), Cd-glutathione (Cd-GSH) and Cd-cysteine spectra had similar pattern, thus hampering the exact determination of the nature of sulfur donor ligands; however, they can be encompassed as thiol groups. Therefore, the distribution of Cd ligands, as results of linear combination fits (LCFs) of Cd L_{III}-edge XANES and µXANES spectra, was described as ratios of Cd-S, Cd-O-P, and Cd-O-C compounds (Figure 3D).

In the S and Cd-enriched areas attributed to the pyrenoid, µXANES analysis revealed that Cd was mainly coordinated by thiol ligands (67 ± 10% and 56 ± 10% for the two presented pyrenoids), but also by carboxyl groups (33 ± 10% and 44 ± 10%). No phosphate ligand was identified in these spots. A pyrenoid consists principally of proteins, mainly RuBisCO, thus µXANES results could indicate cadmium binding to protein thiol groups. Finally, Cd bound to carboxyl groups could be attributed to Cd sequestered to the starch shell around the pyrenoid since µXANES here probed a three-dimensional volume.

XANES measurements of bulk samples showed that Cd- thiol ligands in algae accounted for 31 ± 10% only while Cd- carboxyl groups amounted to 25 ± 10%. The main part of Cd was associated with phosphate ligands (44 ± 10%) suggesting that the calcium polyphosphate granules sequestered an important part of the metal in *C. reinhardtii*. Indeed, these granules were previously probed by µXANES and revealed the sequestration of Cd by phosphate ligands (Penen et al., 2017).

Cadmium promotes carbon incorporation from acetate in starch

In order to investigate the impact of Cd on carbon fixation and to distinguish inorganic and organic carbon sources of *C. reinhardtii*, i.e. CO_2 and acetate, ^{13}C labeled acetate was employed

447 for tracer experiments. *C. reinhardtii* control cells and cells exposed to 70 µM Cd for 48 h in
448 TAP_{EDDHA} medium containing ^{13}C labeled acetate were examined by NanoSIMS (Figure 4).
449 $^{13}C/^{12}C$ ratio maps highlight intracellular areas of carbon resulting from acetate assimilation
450 (high $^{13}C/^{12}C$ ratio) (Figure 4A and B).

451 Two different subcellular regions of interest (ROI) were selected in $^{13}C/^{12}C$ ratio maps (Figure
452 S1) to investigate carbon assimilation: the pyrenoid as organelle of CO_2 fixation and the starch
453 plates as a final storage form of carbon in *C. reinhardtii*. Based on data from ROI in 6 individual
454 control cells and 6 exposed cells (Figure S1), the ^{13}C isotopic enrichment $\delta^{13}C$ was calculated
455 as represented in Figure 4C. Hence, ^{13}C enrichment was found in the pyrenoid, but it did not
456 change significantly under Cd exposure. In contrast, starch plates showed a 5-fold higher ^{13}C
457 enrichment under Cd exposure than in unexposed cells. In particular, the study of carbon
458 isotopic distribution in starch as the final carbon storage form allowed the quantification of
459 carbon assimilation from CO_2 and acetate sources.

460 The determination of $f_{acetate}$ and f_{CO2} in starch granules revealed that, under control conditions,
461 73% of starch carbon came from CO_2 (^{12}C) and 27% from acetate (^{13}C) (RSD ± 9%). In
462 contrast, Cd stress seemed to disturb CO_2 (^{12}C) assimilation which decreased to 39% while
463 acetate (^{13}C) assimilation contributed for 61% of starch carbon (Figure 4D) (RSD ± 13%).
464 Moreover, when the isotopic distribution of starch carbon was combined with the starch
465 concentration previously analyzed (Figure 1D), it appeared that overall CO_2 carbon (^{12}C)
466 assimilation remained limited (1.28 ± 0.18 mmol (^{12}C) g^{-1} in control condition; 1.26 ± 0.43
467 mmol (^{12}C) g^{-1} under Cd exposure) (Figure 4E) relative to the highly increased starch
468 biosynthesis under Cd exposure. In contrast, acetate carbon (^{13}C) assimilation was about 4-fold
469 higher during Cd exposure (0.48 ± 0.15 mmol (^{13}C) g^{-1} under control conditions; 1.99 ± 0.47
470 mmol (^{13}C) g^{-1} under Cd exposure). These results suggest that Cd exposure interfered with CO_2

assimilation due to the Cd fixation in the pyrenoid possibly due to the Cd binding to protein thiol groups.

DISCUSSION

Effect of the culture medium on cell vitality

C. reinhardtii was cultivated in a modified version of TAP medium where EDTA was replaced with EDDHA (TAP_{EDDHA}) in order to increase Cd availability and, at the same time, Cd toxicity. However, under control conditions, this modification induced already a decrease of cell vitality. Indeed, in our previous work (Penen et al., 2017), *C. reinhardtii* grown in classic TAP medium showed a higher growth rate (1.15 ± 0.03 d^{-1}) and a higher production of chlorophyll (10.78 ± 0.38 µg ml^{-1} OD_{730nm}^{-1}) compared to the present study where microalgae have been cultivated in TAP_{EDDHA} medium (Figure 1B, C). These effects of TAP_{EDDHA} medium on cell vitality in control conditions could be explained by changes in the availability of some trace elements compared to the classic TAP medium (Table 1). Indeed, higher availability mainly of zinc but also, to a lesser extent, of copper, and in addition deficiency of cobalt was found in the control TAP_{EDDHA} medium.

Cell response to cadmium stress

Cell vitality results showed that a 70 µM Cd exposure for 48 h induced a decrease of the chlorophyll concentration, which is a well-known sign of photosynthesis impairment (Nagel & Voigt, 1989; Collard & Matagne, 1990; Nagel & Voigt, 1995; Prasad, Drej, Skawińska & Strałka, 1998). The degradation of the chlorophyll pool was concomitant with a growth decrease and an increase of carbon storage in the form of starch. Usually, this stress reaction has been described in *C. reinhardtii* during nitrogen (Ball et al., 1990; Cakmak et al., 2012), phosphorus (Ball et al., 1990) and sulfur (Ball et al., 1990; Cakmak et al., 2012) starvation.

Moreover, Juergens et al. (2015, 2016) showed that starch was accumulated to maintain a carbon pool during N-starvation instead of delaying photoinhibition and oxidative stress due to energetic overflows from photosynthesis. In case of metallic stress, starch storage was reported in *Chlamydomonas acidophila* (Nishikawa, Yamakoshi, Uemura & Tominaga, 2003) exposed to 20 µM Cd where the size of starch plates observed microscopically increased 2.43-fold. Metal stress could thus induce, in an indirect way, symptoms similar to those of nutrient starvation. Working with *C. reinhardtii,* Bräutigam et al. (2011) showed that Cd stress induced the synthesis of thiol polypeptides like phytochelatins, resulting in a decrease in the intracellular concentration of its precursors like glutathione, γ-EC and cysteine leading presumably to a sulfur starvation. Although, sulfur supply by the medium should be sufficient (Bräutigam et al., 2011), an intracellular sulfur deficiency is conceivable. Furthermore, a proteomic study (Gillet, Decottignies, Chardonnet & Maréchal, 2006) revealed that enzymes involved in sulfur metabolism were modified under Cd stress in order to promote the synthesis of phytochelatins.

Cadmium is bound to RuBisCO in pyrenoid and to phosphate in acidocalcisome

For the first time, a pyrenoidal sequestration of Cd and its binding to sulfur ligands were clearly observed in *C. reinhardtii*. In addition, high sulfur and nitrogen content indicated a high protein concentration in the pyrenoid. A model of the impact of Cd sequestration on carbon fixation in *C. reinhardtii* is proposed in Figure 5. Pyrenoids are essentially composed of the protein RuBisCO (Borkhsenious, Mason & Moroney, 1998). They are the place of the carbon fixation from CO_2 via the Calvin cycle (Harris, 1989). Beside RuBisCO, the enzyme RuBisCO-activase is involved in this process (McKay, Gibbs & Vaughn, 1991). Thus, it can be hypothesized that

Cd binding to protein thiol groups interferes with CO_2 fixation in *C. reinhardtii*, for example due to conformational changes caused by cadmium-thiol bonds. Indeed, it has been reported that modifications at cysteines 449 and 459 of the RuBisCO large subunit induce a conformational change and a decrease of its carboxylase activity (Marín-Navarro & Moreno, 2006). Moreover, the RuBisCO large subunit protein is down-regulated under Cd exposure (Gillet et al., 2006). For higher plants, it has been shown that Cd impairs the CO_2 assimilation rate by RuBisCO activity decrease, e.g. in the crop *Lactuca sativa* (Dias et al., 2012) and in *Nicotiana rustica* (Afef, Leila, Donia, Houda & Chiraz, 2011).

In addition, TEM/X-EDS, µXRF and Cd L_{III}-edge XANES measurements have shown that Cd was also coordinated by phosphate ligands and localized in 0.5-1 µm sized vacuoles containing phosphorus and calcium. In our previous work (Penen et al., 2017), cadmium was shown to be localized in vacuoles which were compared to acidocalcisomes due to their specific elemental composition in phosphorus and calcium (Goodenough, Heiss, Roth, Rusch & Lee, 2019; Hong-Hermesdorf et al., 2014; Komine, Eggink, Park & Hoober, 2000; Komine, Park, Wolfe & Hoober, 1996; Ruiz et al., 2001).

CO_2 fixation is impaired by cadmium stress

Cadmium has been shown to disturb the light-dependent part of the photosynthesis (Faller et al., 2005) but no study has previously focused on the impact of Cd on carbon assimilation. *C. reinhardtii* is able to grow photoautotrophically using CO_2, heterotrophically using acetate in the dark and mixotrophically using both carbon sources in the light. In the present study, mixotrophic growth conditions under constant illumination induced carbon storage as starch (Figure 1D). Moreover, NanoSIMS analysis revealed that, carbon from acetate was accumulated in the pyrenoid and in starch granules (Figure 4B). The pathways involved in

542 acetate assimilation as well as the impact of cadmium on these pathways are discussed in the
543 next paragraphs and are represented in Figure 5.

544 The accumulation of carbon from acetate in the pyrenoid can be explained by the assimilation
545 of acetate through the tricarboxylic acid cycle (TCA). Indeed, acetate assimilation starts with
546 its incorporation into acetyl coenzyme A (acetyl-CoA), either directly converted by acetyl-CoA
547 synthetase, or in two steps with the successive action of acetate kinase and phosphate
548 acetyltransferase. Acetyl-CoA is used as substrate in the TCA cycle in mitochondria. The TCA
549 cycle produces ATP as well as NADH and releases the carbon of acetyl-CoA as CO_2 (Johnson
550 & Alric, 2013). Then, the mitochondrial carbonic anhydrase CaH4/5 (Raven, 2001) converts
551 CO_2 in bicarbonate which is carried to the pyrenoid by the CO_2 concentrating mechanism
552 (CCM) (Meyer & Griffiths, 2013). This latter is a combination of active carbon transporters
553 (Burow, Chen, Mouton & Moroney, 1996; Im & Grossman, 2002; Miura et al., 2004; Pollock,
554 Prout, Godfrey, Lemaire & Moroney, 2004), carbonic anhydrases (Moroney et al., 2011)
555 specific to cellular compartments and the soluble proteins (LCIB/LCIC) (Yamano et al., 2010)
556 allowing CO_2 trapping inside the pyrenoid. In the present work, the isotopic ratio of carbon
557 (^{13}C enrichment) inside the pyrenoid was similar under control and exposure conditions (Figure
558 4C) showing that cadmium did not seem to disturb TCA cycle and CCM.

559 Starch biosynthesis involves the successive actions of ADP-glucose pyrophosphorylase
560 (AGPP) and starch synthase (SS) on the final product of the gluconeogenesis pathway (glucose-
561 1-phosphate (G1P)). Carbon from acetate enters gluconeogenesis in two different ways, once
562 incorporated into AcetylCoA. On the one hand, as mentioned in the previous paragraph,
563 AcetylCoA feeds the TCA cycle releasing CO_2. In the chloroplast, the two carbon sources thus
564 share the CO_2 fixation step by RuBisCO into the Calvin cycle pathway. The final product of
565 the Calvin cycle (glyceraldehyde-3-phosphate (G3P)) can enter the gluconeogenesis (Johnson

& Alric, 2013). On the other hand, Acetyl-CoA feeds the glyoxylate cycle which is a TCA cycle where CO_2 releasing steps are by-passed (Johnson & Alric, 2012, 2013) in the cytosol. Indeed, using AcetylCoA and isocitrate as substrates, isocitrate lyase produces glyoxylate and succinate. This latter is successively converted in mitochondria to fumarate, malate, oxaloacetate then phosphoenolpyruvate (PEP) which is exported to cytosol and enters the gluconeogenesis pathway.

C. reinhardtii is able to assimilate inorganic carbon via PEP carboxylation by the two PEP carboxylases CrPpc1/CrPpc2, leading to the production of oxaloacetate (Mamedov, Moellering & Chollet, 2005). However, the algal PEP carboxylase activity is mainly anaplerotic and not photosynthetic (Giordano, Norici, Forssen, Eriksson & Raven, 2003). Although the impact of cadmium on PEPC activity is not established in *C. reinhardtii,* it has been shown that Cd inhibits PEPC activity in higher plants like Miscanthus species (Guo et al., 2016) and Zea mays (Wang, Zhao, Liu, Zhou, & Jin, 2009).

Despite ^{13}C-[1,2] labeling of acetate, our experiments do not allow us to distinguish the pathways taken by acetate carbons to be finally incorporated in starch. However, unlabeled carbon assimilation from CO_2 can only pass by the Calvin cycle. In consequence, after a 48 h Cd exposure, the relative decrease in ^{12}C from 73 to 39% of starch carbon (Figure 4D) shows that carbon fixation through Calvin cycle pathway is limited by Cd stress but not completely inhibited. Hence, the high increase of starch biosynthesis under Cd stress (Figure 1D) is achieved in mixotrophic conditions by an about 4-fold higher carbon assimilation from acetate. However, the overall amount of carbon assimilation from CO_2 into starch remains limited in relation to the increase of starch production (Figure 4E). Moreover, the decrease in chlorophyll concentration (figure 1C) coupled with a massive accumulation of Cd in the pyrenoid (Figures

589 2D, G and 3A) seems to disturb not only the light-dependent reactions (Faller et al., 2005) but
590 also the light-independent reactions of photosynthesis.

591 In unexposed *C. reinhardtii* grown under mixotrophic conditions, 78% of total carbon (Heifetz
592 et al., 2000) has been found to be from CO_2 assimilation which is similar to the 73% of starch
593 carbon originating from CO_2 found in this work. Although Cd exposure and nutrient starvation
594 have a similar impact on starch accumulation, the limitation of CO_2 fixation is specific to Cd
595 stress, since during nitrogen starvation, 65% of starch carbon (Juergens et al., 2016) as well as
596 80% of total carbon (Juergens et al., 2016) are taken from an inorganic carbon source. In
597 addition, enzymes involved in Calvin cycle have been shown to be down-regulated under Cd
598 stress (phosphoglycerate kinase, ribose-5phosphate isomerase) while enzymes involved in
599 acetate assimilation were up-regulated as for the isocitrate lyase (Gillet et al., 2006) involved
600 in the glyoxylate cycle or the phosphoglycerate mutase (Gillet et al., 2006) taking part in
601 gluconeogenesis.

602 Using NanoSIMS in combination with ^{13}C-labeled acetate it was possible to detect, localize,
603 and quantify ^{13}C-labeled starch as end product within the cells. Although these are important
604 results, the limitation of this approach is, that between the acetate substrate and the end product
605 no other metabolites of the carbon metabolism pathway during cadmium stress were measured.
606 A metabolomic or a fluxomic approach would be necessary to complete our results with regard
607 to the overall carbon fixation and metabolism pathway involved during cadmium stress in *C.*
608 *reinhardtii*.

609 In conclusion, the present work shows that cadmium clearly impairs carbon assimilation in *C.*
610 *reinhardtii* grown in mixotrophic conditions. Due to the pyrenoidal sequestration of Cd, CO_2
611 fixation is limited during Cd exposure whereas acetate assimilation is favored. Mixotrophy
612 could thus allow phytoplankton surviving toxic metal pollution events. Although mixotrophy

seems to render aquatic ecosystems more resistant, the alteration of CO_2 fixation by toxic metals could contribute to the unbalance of the biogeochemical carbon cycle.

ACKNOWLEDGEMENTS

The work was supported by funding from the French 'Ministère de l'Enseignement Supérieur et de la Recherche' via the projects ANR-11-EQPX-0027 MARSS and ANR-10-INBS-04 FranceBioImaging, and a PhD fellowship for F.P. Furthermore, this work was supported by the bilateral (German-French) DAAD - Campus France program PROCOPE funded by the German 'Bundesministerium für Bildung und Forschung (BMBF)', the French 'Ministère des Affaires étrangères et du développement International (MAEDI)' and 'Ministère de l'Education nationale, de l'Enseignement supérieur et de la Recherche (MENESR)'. We also thank ESRF (Grenoble, France) for the provision of beamtime on ID21 beamline. The microscopy was done in the Bordeaux Imaging Center, a service unit of the CNRS-INSERM and Bordeaux University, member of the national infrastructure France BioImaging. The authors thank kindly Prof. U. Johanningmeier and Dr. I. Bertalan from the University Halle-Wittenberg (Germany) for providing *C. reinhardtii* wild type strain (11/32b).

CONFLICT OF INTEREST

The authors declare no conflict of interests.

REFERENCES

Adams, M. S., Dillon, C. T., Vogt, S., Lai, B., Stauber, J., & Jolley, D. F. (2016). Copper Uptake, Intracellular Localization, and Speciation in Marine Microalgae Measured by Synchrotron Radiation X-ray Fluorescence and Absorption Microspectroscopy. *Environmental Science & Technology*, *50*(16), 8827–8839.

Afef, N.-H., Leila, S., Donia, B., Houda, G., & Chiraz, C.-H. (2011). Relationship between physiological and biochemical effects of cadmium toxicity in Nicotiana rustica. *American Journal of Plant Physiology*, *6*(6), 294–303.

Aguilera, A., & Amils, R. (2005). Tolerance to cadmium in Chlamydomonas sp. (Chlorophyta) strains isolated from an extreme acidic environment, the Tinto River (SW, Spain). *Aquatic Toxicology*, *75*(4), 316–329.

Aksmann, A., Pokora, W., Baścik-Remisiewicz, A., Dettlaff-Pokora, A., Wielgomas, B., Dziadziuszko, M., & Tukaj, Z. (2014). Time-dependent changes in antioxidative enzyme expression and photosynthetic activity of Chlamydomonas reinhardtii cells under acute exposure to cadmium and anthracene. *Ecotoxicology and Environmental Safety*, *110*, 31–40.

Arnon, D. I. (1949). Copper Enzymes in Isolated Chloroplasts. Polyphenoloxidase in Beta Vulgaris. *Plant Physiology*, *24*(1), 1–15.

Badger, M. R., Andrews, T. J., Whitney, S. M., Ludwig, M., Yellowlees, D. C., Leggat, W., & Price, G. D. (1998). The diversity and coevolution of Rubisco, plastids, pyrenoids, and chloroplast-based CO2-concentrating mechanisms in algae. *Canadian Journal of Botany*, *76*(6), 1052–1071.

Ball, S. G., Dirick, L., Decq, A., Martiat, J.-C., & Matagne, R. (1990). Physiology of starch storage in the monocellular alga Chlamydomonas reinhardtii. *Plant Science*, *66*(1), 1–9.

Borkhsenious, O. N., Mason, C. B., & Moroney, J. V. (1998). The Intracellular Localization of Ribulose-1,5-Bisphosphate Carboxylase/Oxygenase in Chlamydomonas reinhardtii. *Plant Physiology*, *116*(4), 1585–1591.

Bräutigam, A., Schaumlöffel, D., Krauss, G.-J., & Wesenberg, D. (2009). Analytical approach for characterization of cadmium-induced thiol peptides—a case study using Chlamydomonas reinhardtii. *Analytical and Bioanalytical Chemistry*, *395*(6), 1737–1747.

Bräutigam, A., Schaumlöffel, D., Preud'Homme, H., Thondorf, I., & Wesenberg, D. (2011). Physiological characterization of cadmium-exposed Chlamydomonas reinhardtii. *Plant, Cell and Environment*, *34*(12), 2071–2082.

Burkholder, J. M., Glibert, P. M., & Skelton, H. M. (2008). Mixotrophy, a major mode of nutrition for harmful algal species in eutrophic waters. *Harmful Algae*, *8*(1), 77–93.

Burow, M. D., Chen, Z.-Y., Mouton, T. M., & Moroney, J. V. (1996). Isolation of cDNA clones of genes induced upon transfer of Chlamydomonas reinhardtii cells to low CO2. *Plant Molecular Biology*, *31*(2), 443–448.

Cakmak, T., Angun, P., Demiray, Y. E., Ozkan, A. D., Elibol, Z., & Tekinay, T. (2012). Differential effects of nitrogen and sulfur deprivation on growth and biodiesel feedstock production of Chlamydomonas reinhardtii. *Biotechnology and Bioengineering*, *109*(8), 1947–1957.

Campbell, P. G. C. (2006). Cadmium-A priority pollutant. *Environmental Chemistry*, *3*(6), 387–388.

Caron, D. A. (2016). Mixotrophy stirs up our understanding of marine food webs. *Proceedings of the National Academy of Sciences*, *113*(11), 2806–2808.

681 Clode, P. L., Stern, R. A., & Marshall, A. T. (2007). Subcellular imaging of isotopically labeled
682 carbon compounds in a biological sample by ion microprobe (NanoSIMS). *Microscopy*
683 *Research and Technique*, *70*(3), 220–229.
684 Collard, J. M., & Matagne, R. F. (1990). Isolation and genetic analysis of Chlamydomonas
685 reinhardtii strains resistant to cadmium. *Applied and Environmental Microbiology*,
686 *56*(7), 2051–2055.
687 Cotte, M., Pouyet, E., Salomé, M., Rivard, C., Nolf, W. D., Castillo-Michel, H., Fabris, T.,
688 Monico, L., Janssens, K., Wang, T., Sciau, P., Verger, L., Cormier, L., Dargaud, O.,
689 Brun, E., Bugnazet, D., Fayard, B., Hesse, B., Real, A.E.P., Veronesi, G., Langlois, J.,
690 Balcar, N., Vandenberghe, Y., Solé, V.A., Kieffer, J., Barrett, R., Cohen, C., Cornu, C.,
691 Baker, R., Gagliardini, E., Papillon, E. & Susini, J. (2017). The ID21 X-ray and infrared
692 microscopy beamline at the ESRF: status and recent applications to artistic materials.
693 *Journal of Analytical Atomic Spectrometry*, *32*(3), 477–493.
694 Croteau, M.-N., Luoma, S. N., & Stewart, A. R. (2005). Trophic transfer of metals along
695 freshwater food webs: Evidence of cadmium biomagnification in nature. *Limnology*
696 *and Oceanography*, *50*(5), 1511–1519.
697 Delrue, B., Fontaine, T., Routier, F., Decq, A., Wieruszeski, J. M., Van Den Koornhuyse, N.,
698 Maddelein, M.L., Fournet, B. & Ball, S. (1992). Waxy Chlamydomonas reinhardtii:
699 monocellular algal mutants defective in amylose biosynthesis and granule-bound starch
700 synthase activity accumulate a structurally modified amylopectin. *Journal of*
701 *Bacteriology*, *174*(11), 3612–3620.
702 Dent, R. M., Han, M., & Niyogi, K. K. (2001). Functional genomics of plant photosynthesis in
703 the fast lane using Chlamydomonas reinhardtii. *Trends in Plant Science*, *6*(8), 364–371.

Dias, M. C., Monteiro, C., Moutinho-Pereira, J., Correia, C., Gonçalves, B., & Santos, C. (2012). Cadmium toxicity affects photosynthesis and plant growth at different levels. *Acta Physiologiae Plantarum*, *35*(4), 1281–1289.

Ellis, R. J. (1979). The most abundant protein in the world. *Trends in Biochemical Sciences*, *4*(11), 241–244.

Faller, P., Kienzler, K., & Krieger-Liszkay, A. (2005). Mechanism of Cd2+ toxicity: Cd2+ inhibits photoactivation of Photosystem II by competitive binding to the essential Ca2+ site. *Biochimica et Biophysica Acta (BBA) - Bioenergetics*, *1706*(1–2), 158–164.

Field, C. B., Behrenfeld, M. J., Randerson, J. T., & Falkowski, P. (1998). Primary Production of the Biosphere: Integrating Terrestrial and Oceanic Components. *Science*, *281*(5374), 237–240.

Gao, D., Huang, X., & Tao, Y. (2016). A critical review of NanoSIMS in analysis of microbial metabolic activities at single-cell level. *Critical Reviews in Biotechnology*, *36*(5), 884–890.

Gekeler, W., Grill, E., Winnacker, E.-L., & Zenk, M. H. (1988). Algae sequester heavy metals via synthesis of phytochelatin complexes. *Archives of Microbiology*, *150*(2), 197–202.

Gillet, S., Decottignies, P., Chardonnet, S., & Maréchal, P. L. (2006). Cadmium response and redoxin targets in Chlamydomonas reinhardtii: a proteomic approach. *Photosynthesis Research*, *89*(2–3), 201–211.

Giordano, M., Norici, A., Forssen, M., Eriksson, M., & Raven, J. A. (2003). An Anaplerotic Role for Mitochondrial Carbonic Anhydrase in Chlamydomonas reinhardtii. *Plant Physiology*, *132*(4), 2126–2134.

Goodenough, U., Heiss, A. A., Roth, R., Rusch, J., & Lee, J.-H. (2019). Acidocalcisomes: Ultrastructure, Biogenesis, and Distribution in Microbial Eukaryotes. *Protist*, *170*(3), 287–313.

729 Goodenough, U. W., Shames, B., Small, L., Saito, T., Crain, R. C., Sanders, M. A., &
730 Salisbury, J. L. (1993). The role of calcium in the Chlamydomonas reinhardtii mating
731 reaction. *Journal of Cell Biology*, *121*(2), 365–374.
732 Goto, K., & Johnson, C. H. (1995). Is the cell division cycle gated by a circadian clock? The
733 case of Chlamydomonas reinhardtii. *The Journal of Cell Biology*, *129*(4), 1061–1069.
734 Guo, H., Hong, C., Chen, X., Xu, Y., Liu, Y., Jiang, D., & Zheng, B. (2016). Different Growth
735 and Physiological Responses to Cadmium of the Three Miscanthus Species. *PLOS*
736 *ONE*, *11*(4), e0153475.
737 Gustafsson, J., Petter. (2013). Visual MINTEQ | Visual MINTEQ – a free equilibrium
738 speciation model. Retrieved March 31, 2017, from http://vminteq.lwr.kth.se/.
739 Hanikenne, M. (2003). Chlamydomonas reinhardtii as a eukaryotic photosynthetic model for
740 studies of heavy metal homeostasis and tolerance. *New Phytologist*, *159*(2), 331–340.
741 Harris, E. H. (1989). *The Chlamydomonas Sourcebook: Introduction to Chlamydomonas and*
742 *Its Laboratory Use*. Academic Press, Inc. San Diego.
743 Hartmann, M., Grob, C., Tarran, G. A., Martin, A. P., Burkill, P. H., Scanlan, D. J., & Zubkov,
744 M. V. (2012). Mixotrophic basis of Atlantic oligotrophic ecosystems. *Proceedings of*
745 *the National Academy of Sciences*, *109*(15), 5756–5760.
746 Heifetz, P. B., Förster, B., Osmond, C. B., Giles, L. J., & Boynton, J. E. (2000). Effects of
747 Acetate on Facultative Autotrophy inChlamydomonas reinhardtii Assessed by
748 Photosynthetic Measurements and Stable Isotope Analyses. *Plant Physiology*, *122*(4),
749 1439–1446.
750 Hong-Hermesdorf, A., Miethke, M., Gallaher, S. D., Kropat, J., Dodani, S. C., Chan, J.,
751 Barupala, D., Domaille, D.W., Shirasaki, D.I., Loo, J.A., Weber, P.K., Pett-Ridge, J.,
752 Stemmler, T.L., Chang, C.J. & Merchant, S. S. (2014). Subcellular metal imaging

identifies dynamic sites of Cu accumulation in Chlamydomonas. *Nature Chemical Biology*, *10*(12): 1034–1042.

Hoppe, P., Cohen, S., & Meibom, A. (2013). NanoSIMS: Technical Aspects and Applications in Cosmochemistry and Biological Geochemistry. *Geostandards and Geoanalytical Research*, *37*(2), 111–154.

Huguet, S., Bert, V., Laboudigue, A., Barthès, V., Isaure, M.-P., Llorens, I., Schat, H. & Sarret, G. (2012). Cd speciation and localization in the hyperaccumulator Arabidopsis halleri. *Environmental and Experimental Botany*, *82*, 54–65.

Ikemoto, T., Tu, N. P. C., Okuda, N., Iwata, A., Omori, K., Tanabe, S., Tuyen, B.C. & Takeuchi, I. (2008). Biomagnification of Trace Elements in the Aquatic Food Web in the Mekong Delta, South Vietnam Using Stable Carbon and Nitrogen Isotope Analysis. *Archives of Environmental Contamination and Toxicology*, *54*(3), 504–515.

Im, C. S., & Grossman, A. R. (2002). Identification and regulation of high light-induced genes in Chlamydomonas reinhardtii. *The Plant Journal*, *30*(3), 301–313.

Isaure, M.-P., Fayard, B., Sarret, G., Pairis, S., & Bourguignon, J. (2006). Localization and chemical forms of cadmium in plant samples by combining analytical electron microscopy and X-ray spectromicroscopy. *Spectrochimica Acta Part B: Atomic Spectroscopy*, *61*(12), 1242–1252.

Isaure, M.-P., Huguet, S., Meyer, C.-L., Castillo-Michel, H., Testemale, D., Vantelon, D., Saumitou-Laprade, P., Verbruggen, N. & Sarret, G. (2015). Evidence of various mechanisms of Cd sequestration in the hyperaccumulator Arabidopsis halleri, the non-accumulator Arabidopsis lyrata, and their progenies by combined synchrotron-based techniques. *Journal of Experimental Botany*, *66*(11), 3201–3214.

776 Johnson, X., & Alric, J. (2012). Interaction between Starch Breakdown, Acetate Assimilation,
777 and Photosynthetic Cyclic Electron Flow in Chlamydomonas reinhardtii. *Journal of*
778 *Biological Chemistry*, *287*(31), 26445–26452.
779 Johnson, X., & Alric, J. (2013). Central Carbon Metabolism and Electron Transport in
780 Chlamydomonas reinhardtii: Metabolic Constraints for Carbon Partitioning between
781 Oil and Starch. *Eukaryotic Cell*, *12*(6), 776–793.
782 Juergens, M. T., Deshpande, R. R., Lucker, B. F., Park, J.-J., Wang, H., Gargouri, M., Holguin,
783 F.O., Disbrow, B., Schaub, T., Skepper, J.N., Kramer, D.M., Gang, D.R., Hicks, L.M.
784 & Shachar-Hill, Y. (2015). The Regulation of Photosynthetic Structure and Function
785 during Nitrogen Deprivation in Chlamydomonas reinhardtii. *Plant Physiology*, *167*(2),
786 558–573.
787 Juergens, M. T., Disbrow, B., & Shachar-Hill, Y. (2016). The Relationship of Triacylglycerol
788 and Starch Accumulation to Carbon and Energy Flows during Nutrient Deprivation in
789 Chlamydomonas reinhardtii. *Plant Physiology*, *171*(4), 2445–2457.
790 Komine, Y., Eggink, L. L., Park, H., & Hoober, J. K. (2000). Vacuolar granules in
791 Chlamydomonas reinhardtii: polyphosphate and a 70-kDa polypeptide as major
792 components. *Planta*, *210*(6), 897–905.
793 Komine, Y., Park, H., Wolfe, G. R., & Hoober, J. K. (1996). Secretory granules in the
794 cytoplasm of a wall-less mutant of Chlamydomonas reinhardtii contain processed light-
795 harvesting complex apoproteins and HSP70. *Journal of Photochemistry and*
796 *Photobiology B: Biology*, *36*(3), 301–306.
797 Kopp, C., Domart-Coulon, I., Escrig, S., Humbel, B. M., Hignette, M., & Meibom, A. (2015).
798 Subcellular Investigation of Photosynthesis-Driven Carbon Assimilation in the
799 Symbiotic Reef Coral Pocillopora damicornis. *mBio*, *6*(1), e02299-14.

800 Lavoie, M., Fortin, C., & Campbell, P. G. C. (2012). Influence of essential elements on
801 cadmium uptake and toxicity in a unicellular green alga: The protective effect of trace
802 zinc and cobalt concentrations. *Environmental Toxicology and Chemistry*, *31*(7), 1445–
803 1452.
804 Lechene, C., Hillion, F., McMahon, G., Benson, D., Kleinfeld, A. M., Kampf, J. P., Distel, D.,
805 Luyten, Y., Bonventre, J., Hentschel, D., Park, K.M., Ito, S., Schwartz, M., Benichou,
806 G. & Slodzian, G. (2006). High-resolution quantitative imaging of mammalian and
807 bacterial cells using stable isotope mass spectrometry. *Journal of Biology*, *5*, 20.
808 Lee, T.-M., Lai, H.-Y., & Chen, Z.-S. (2004). Effect of chemical amendments on the
809 concentration of cadmium and lead in long-term contaminated soils. *Chemosphere*,
810 *57*(10), 1459–1471.
811 Leonardo, T., Farhi, E., Boisson, A.-M., Vial, J., Cloetens, P., Bohic, S., & Rivasseau, C.
812 (2014). Determination of elemental distribution in green micro-algae using synchrotron
813 radiation nano X-ray fluorescence (SR-nXRF) and electron microscopy techniques –
814 subcellular localization and quantitative imaging of silver and cobalt uptake by
815 Coccomyxa actinabiotis. *Metallomics*, *6*(2), 316–329.
816 Leonardo, T., Farhi, E., Pouget, S., Motellier, S., Boisson, A.-M., Banerjee, D., Rébeillé, F.,
817 den Auwer, C. & Rivasseau, C. (2016). Silver Accumulation in the Green Microalga
818 Coccomyxa actinabiotis: Toxicity, in Situ Speciation, and Localization Investigated
819 Using Synchrotron XAS, XRD, and TEM. *Environmental Science & Technology*,
820 *50*(1), 359–367.
821 Lindsay, W. L. (1979). *Chemical equilibria in soils*. John Wiley & Sons, New York.
822 Macfie, S. M., Tarmohamed, Y., & Welbourn, P. M. (1994). Effects of cadmium, cobalt,
823 copper, and nickel on growth of the green alga Chlamydomonas reinhardtii: The

influences of the cell wall and pH. *Archives of Environmental Contamination and Toxicology*, *27*(4), 454–458.

Mackinder, L. C. M., Meyer, M. T., Mettler-Altmann, T., Chen, V. K., Mitchell, M. C., Caspari, O., Rosenzweig, E.S.F., Pallesen, L., Reeves, G., Itakura, A., Roth, R., Sommer, F., Geimer, S., Mühlhaus, T., Schroda, M., Goodenough, U., Stitt, M., Griffiths, H. & Jonikas, M. C. (2016). A repeat protein links Rubisco to form the eukaryotic carbon-concentrating organelle. *Proceedings of the National Academy of Sciences*, *113*(21), 5958–5963.

Malherbe, J., Penen, F., Isaure, M.-P., Frank, J., Hause, G., Dobritzsch, D., Gontier, E., Horréard, F., Hillion, F. & Schaumlöffel, D. (2016). A New Radio Frequency Plasma Oxygen Primary Ion Source on Nano Secondary Ion Mass Spectrometry for Improved Lateral Resolution and Detection of Electropositive Elements at Single Cell Level. *Analytical Chemistry*, *88*(14), 7130–7136.

Mamedov, T. G., Moellering, E. R., & Chollet, R. (2005). Identification and expression analysis of two inorganic C- and N-responsive genes encoding novel and distinct molecular forms of eukaryotic phosphoenolpyruvate carboxylase in the green microalga Chlamydomonas reinhardtii. *The Plant Journal*, *42*(6), 832–843.

Marín-Navarro, J., & Moreno, J. (2006). Cysteines 449 and 459 modulate the reduction–oxidation conformational changes of ribulose 1·5-bisphosphate carboxylase/oxygenase and the translocation of the enzyme to membranes during stress. *Plant, Cell & Environment*, *29*(5), 898–908.

McKay, R. M. ., Gibbs, S. P., & Vaughn, K. C. (1991). RuBisCo activase is present in the pyrenoid of green algae. *Protoplasma*, (162), 38–45.

Merchant, S. S., Allen, M. D., Kropat, J., Moseley, J. L., Long, J. C., Tottey, S., & Terauchi, A. M. (2006). Between a rock and a hard place: Trace element nutrition in

Chlamydomonas. *Biochimica et Biophysica Acta (BBA) - Molecular Cell Research*, *1763*(7), 578–594.

Merchant, S. S., Kropat, J., Liu, B., Shaw, J., & Warakanont, J. (2012). TAG, You're it! Chlamydomonas as a reference organism for understanding algal triacylglycerol accumulation. *Current Opinion in Biotechnology*, *23*(3), 352–363.

Merchant, S. S., Prochnik, S. E., Vallon, O., Harris, E. H., Karpowicz, S. J., Witman, G. B., … Grossman, A. R. (2007). The Chlamydomonas Genome Reveals the Evolution of Key Animal and Plant Functions. *Science*, *318*(5848), 245–250.

Meyer, M., & Griffiths, H. (2013). Origins and diversity of eukaryotic CO2-concentrating mechanisms: lessons for the future. *Journal of Experimental Botany*, *64*(3), 769–786.

Miura, K., Yamano, T., Yoshioka, S., Kohinata, T., Inoue, Y., Taniguchi, F., Asamizu, E., Nakamura, Y., Tabata, S., Yamato, K.T., Ohyama, K. & Fukuzawa, H. (2004). Expression Profiling-Based Identification of CO2-Responsive Genes Regulated by CCM1 Controlling a Carbon-Concentrating Mechanism in Chlamydomonas reinhardtii. *Plant Physiology*, *135*(3), 1595–1607.

Moore, K. L., Schröder, M., Lombi, E., Zhao, F.-J., McGrath, S. P., Hawkesford, M. J., Shewry, P.R. & Grovenor, C. R. M. (2010). NanoSIMS analysis of arsenic and selenium in cereal grain. *New Phytologist*, *185*(2), 434–445.

Moore, K. L., Schröder, M., Wu, Z., Martin, B. G. H., Hawes, C. R., McGrath, S. P., Hawkesford, M.J., Ma, J.F., Zhao, F.-J. & Grovenor, C. R. M. (2011). High-Resolution Secondary Ion Mass Spectrometry Reveals the Contrasting Subcellular Distribution of Arsenic and Silicon in Rice Roots. *Plant Physiology*, *156*(2), 913–924.

Moore, K. L., Zhao, F.-J., Gritsch, C. S., Tosi, P., Hawkesford, M. J., McGrath, S. P., Tosi, P., Hawkesford, M.J., McGrath, S.P., Shewry, P.R. & Grovenor, C. R. M. (2012).

873 Localisation of iron in wheat grain using high resolution secondary ion mass
874 spectrometry. *Journal of Cereal Science*, *55*(2), 183–187.
875 Moroney, J. V., Ma, Y., Frey, W. D., Fusilier, K. A., Pham, T. T., Simms, T. A., DiMario, R.J.,
876 Yang, J. & Mukherjee, B. (2011). The carbonic anhydrase isoforms of Chlamydomonas
877 reinhardtii: intracellular location, expression, and physiological roles. *Photosynthesis*
878 *Research*, *109*(1–3), 133–149.
879 Nagel, K., & Voigt, J. (1989). In Vitro Evolution and Preliminary Characterization of a
880 Cadmium-Resistant Population of Chlamydomonas reinhardtii. *Applied and*
881 *Environmental Microbiology*, *55*(2), 526–528.
882 Nagel, K., & Voigt, J. (1995). Impaired photosynthesis in a cadmium-tolerant Chlamydomonas
883 mutant strain. *Microbiological Research*, *150*(1), 105–110.
884 Nishikawa, K., Yamakoshi, Y., Uemura, I., & Tominaga, N. (2003). Ultrastructural changes in
885 Chlamydomonas acidophila (Chlorophyta) induced by heavy metals and polyphosphate
886 metabolism. *FEMS Microbiology Ecology*, *44*(2), 253–259.
887 Ortega, R., Devès, G., & Carmona, A. (2009). Bio-metals imaging and speciation in cells using
888 proton and synchrotron radiation X-ray microspectroscopy. *Journal of The Royal*
889 *Society Interface*, *6*(Suppl 5), S649–S658.
890 O'Toole, E. T. (2010). *Chlamydomonas. Cryopreparation methods for the 3-D analysis of*
891 *cellular organelles*. *Methods Cellular Biology*, 96, 71–91.
892 Park, J.-J., Wang, H., Gargouri, M., Deshpande, R. R., Skepper, J. N., Holguin, F. O., Juergens,
893 M.T., Shachar-Hill, Y., Hicks, L.M. & Gang, D. R. (2015). The response of
894 Chlamydomonas reinhardtii to nitrogen deprivation: a systems biology analysis. *The*
895 *Plant Journal*, *81*(4), 611–624.
896 Penen, F., Isaure, M. P., Dobritzsch, D., Bertalan, I., Castillo-Michel, H., Proux, O., Gontier,
897 E., Le Coustumer, P. & Schaumlöffel, D. (2017). Pools of cadmium in Chlamydomonas

reinhardtii revealed by chemical imaging and XAS spectroscopy. *Metallomics*,9, 910-923.

Penen, F., Malherbe, J., Isaure, M.-P., Dobritzsch, D., Bertalan, I., Gontier, E., Le Coustumer, P. & Schaumlöffel, D. (2016). Chemical bioimaging for the subcellular localization of trace elements by high contrast TEM, TEM/X-EDS, and NanoSIMS. *Journal of Trace Elements in Medicine and Biology*, *37*, 62–68.

Pollock, S. V., Prout, D. L., Godfrey, A. C., Lemaire, S. D., & Moroney, J. V. (2004). The Chlamydomonas reinhardtii proteins Ccp1 and Ccp2 are required for long-term growth, but are not necessary for efficient photosynthesis, in a low-CO2 environment. *Plant Molecular Biology*, *56*(1), 125–132.

Prasad, M. N. V., Drej, K., Skawińska, A., & Strałka, K. (1998). Toxicity of Cadmium and Copper in Chlamydomonas reinhardtii Wild-Type (WT 2137) and Cell Wall Deficient Mutant Strain (CW 15). *Bulletin of Environmental Contamination and Toxicology*, *60*(2), 306–311.

Ramani, S., Dragun, Z., Kapetanović, D., Kostov, V., Jordanova, M., Erk, M., & Hajrulai-Musliu, Z. (2014). Surface Water Characterization of Three Rivers in the Lead/Zinc Mining Region of Northeastern Macedonia. *Archives of Environmental Contamination and Toxicology*, *66*(4), 514–528.

Ravel, B., & Newville, M. (2005). *ATHENA* , *ARTEMIS* , *HEPHAESTUS* : data analysis for X-ray absorption spectroscopy using *IFEFFIT*. *Journal of Synchrotron Radiation*, *12*(4), 537–541.

Raven, J. A. (2001). A role for mitochondrial carbonic anhydrase in limiting CO2 leakage from low CO2-grown cells of Chlamydomonas reinhardtii. *Plant, Cell & Environment*, *24*(2), 261–265.

Rochaix, J.-D., M. Goldschmidt-Clermont & Merchant, S. (1998). *The Molecular Biology of Chloroplasts and Mitochondria in Chlamydomonas*. Kluwer Academic Publishers, Dordrecht, The Netherlands.

Roschzttardtz, H., Grillet, L., Isaure, M.-P., Conéjéro, G., Ortega, R., Curie, C., & Mari, S. (2011). Plant Cell Nucleolus as a Hot Spot for Iron. *Journal of Biological Chemistry*, *286*(32), 27863–27866.

Rouleau, C., Gobeil, C., & Tjlve, H. (2006). Cadmium accumulation in coastal demersal fish. *Marine Ecology Progress Series*, *311*, 131–143.

Ruiz, F. A., Marchesini, N., Seufferheld, M., Govindjee, & Docampo, R. (2001). The Polyphosphate Bodies of Chlamydomonas reinhardtii Possess a Proton-pumping Pyrophosphatase and Are Similar to Acidocalcisomes. *Journal of Biological Chemistry*, *276*(49), 46196–46203.

Sarret, G., Smits, E. A. H. P., Michel, H. C., Isaure, M. P., Zhao, F. J. & Tappero, R. (2013). Chapter One - Use of Synchrotron-Based Techniques to Elucidate Metal Uptake and Metabolism in Plants. In D. L. Sparks (Ed.), *Advances in Agronomy* (pp. 1–82).

Schaumlöffel, D., Hutchinson, R., Malherbe, J., Le Coustumer, P., Gontier, E. & Isaure, M.-P. (2016), Novel Methods for Bioimaging Including LA-ICP-MS, NanoSIMS, TEM/X-EDS, and SXRF, In: Metallomics: Analytical Techniques and Speciation Methods,ed. Michalke, B., John Wiley and Sons, ISBN 978-3-527-33969-3, Wiley-VCH Verlag GmbH, Weinheim, pp. 83-116

Signa, G., Mazzola, A., Tramati, C. D., & Vizzini, S. (2017). Diet and habitat use influence Hg and Cd transfer to fish and consequent biomagnification in a highly contaminated area: Augusta Bay (Mediterranean Sea). *Environmental Pollution*, *230*, 394–404.

945 Silflow, C. D., & Lefebvre, P. A. (2001). Assembly and Motility of Eukaryotic Cilia and
946 Flagella. Lessons from Chlamydomonas reinhardtii. *Plant Physiology*, *127*(4), 1500–
947 1507.
948 Simmons, R. W., Pongsakul, P., Saiyasitpanich, D., & Klinphoklap, S. (2005). Elevated levels
949 of cadmium and zinc in paddy soils and elevated levels of cadmium in rice grain
950 downstream of a zinc mineralized area in Thailand: implications for public health.
951 *Environmental Geochemistry and Health*, *27*(5–6), 501–511.
952 Singh, H., Shukla, M. R., Chary, K. V. R., & Rao, B. J. (2014). Acetate and Bicarbonate
953 Assimilation and Metabolite Formation in Chlamydomonas reinhardtii: A 13C-NMR
954 Study. *PLOS ONE*, *9*(9), e106457.
955 Solé, V. A., Papillon, E., Cotte, M., Walter, P., & Susini, J. (2007). A multiplatform code for
956 the analysis of energy-dispersive X-ray fluorescence spectra. *Spectrochimica Acta Part*
957 *B: Atomic Spectroscopy*, *62*(1), 63–68.
958 Stoiber, T. L., Shafer, M. M., & Armstrong, D. E. (2012). Relationships between surface-bound
959 and internalized copper and cadmium and toxicity in Chlamydomonas reinhardtii.
960 *Environmental Toxicology and Chemistry*, *31*(2), 324–335.
961 Terrado, R., Pasulka, A. L., Lie, A. A.-Y., Orphan, V. J., Heidelberg, K. B., & Caron, D. A.
962 (2017). Autotrophic and heterotrophic acquisition of carbon and nitrogen by a
963 mixotrophic chrysophyte established through stable isotope analysis. *The ISME*
964 *Journal*, *11*(9), 2022–2034.
965 Vega, J. M., Garbayo, I., Domínguez, M. J., & Vigara, J. (2006). Effect of abiotic stress on
966 photosynthesis and respiration in Chlamydomonas reinhardtii: Induction of oxidative
967 stress. *Enzyme and Microbial Technology*, *40*(1), 163–167.

968 Voigt, J., & Nagel, K. (2002). The donor side of photosystem II is impaired in a Cd2+-tolerant
969 mutant strain of the unicellular green algaChlamydomonas reinhardtii. *Journal of Plant*
970 *Physiology*, *159*(9), 941–950.
971 Voigt, J., Nagel, K., & Wrann, D. (1998). A Cadmium-tolerant Chlamydomonas Mutant Strain
972 Impaired in Photosystem II Activity. *Journal of Plant Physiology*, *153*(5–6), 566–573.
973 Wang, H., Zhao, S. C., Liu, R. L., Zhou, W., & Jin, J. Y. (2009). Changes of photosynthetic
974 activities of maize (Zea mays L.) seedlings in response to cadmium stress.
975 *Photosynthetica*, *47*(2), 277–283.
976 Wang, S., Lv, J., Ma, J., & Zhang, S. (2016). Cellular internalization and intracellular
977 biotransformation of silver nanoparticles in Chlamydomonas reinhardtii.
978 *Nanotoxicology*, *10*(8), 1129–1135.
979 Ward, B. A., & Follows, M. J. (2016). Marine mixotrophy increases trophic transfer efficiency,
980 mean organism size, and vertical carbon flux. *Proceedings of the National Academy of*
981 *Sciences*, *113*(11), 2958–2963.
982 Worden, A. Z., Follows, M. J., Giovannoni, S. J., Wilken, S., Zimmerman, A. E., & Keeling,
983 P. J. (2015). Rethinking the marine carbon cycle: Factoring in the multifarious lifestyles
984 of microbes. *Science*, *347*(6223), 1257594.
985 Xue, H., & Sigg, L. (1998). Cadmium speciation and complexation by natural organic ligands
986 in fresh water. *Analytica Chimica Acta*, *363*(2–3), 249–259.
987 Yamano, T., Tsujikawa, T., Hatano, K., Ozawa, S.-I., Takahashi, Y., & Fukuzawa, H. (2010).
988 Light and low-CO2-dependent LCIB-LCIC complex localization in the chloroplast
989 supports the carbon-concentrating mechanism in Chlamydomonas reinhardtii. *Plant &*
990 *Cell Physiology*, *51*(9), 1453–1468.

991

TABLES

Table 1: Comparison of ion availability in classic TAP medium and TAP_{EDDHA} medium.

	Free ion concentrations (M)			
	TAP		TAP_{EDDHA}	
Metal ions	Control	70 µM Cd	Control	70 µM Cd
Ca^{2+}	$2.5\ 10^{-5}$	$2.6\ 10^{-5}$	$2.6\ 10^{-5}$	$2.6\ 10^{-5}$
Mg^{2+}	$3.1\ 10^{-4}$	$3.1\ 10^{-4}$	$3.1\ 10^{-4}$	$3.1\ 10^{-4}$
Fe^{2+}	$5.6\ 10^{-9}$	$5.0\ 10^{-7}$	-	-
Fe^{3+}	-	-	$1.1\ 10^{-22}$	$1.2\ 10^{-22}$
Zn^{2+}	$2.4\ 10^{-10}$	$3.0\ 10^{-6}$	$3.1\ 10^{-6}$	$3.1\ 10^{-6}$
Cu^{2+}	$6.5\ 10^{-14}$	$6.1\ 10^{-10}$	$6.9\ 10^{-12}$	$7.5\ 10^{-12}$
Co^{2+}	$1.5\ 10^{-11}$	$2.0\ 10^{-7}$	$5.6\ 10^{-15}$	$4.7\ 10^{-15}$
Mn^{2+}	$10.7\ 10^{-10}$	$8.0\ 10^{-10}$	$8.3\ 10^{-10}$	$8.4\ 10^{-10}$
MoO_4^{2-}	$5.6\ 10^{-6}$	$1.1\ 10^{-8}$	$5.6\ 10^{-6}$	$1.1\ 10^{-9}$
Cd^{2+}	-	$2.1\ 10^{-6}$	-	$2.0\ 10^{-5}$

FIGURE CAPTIONS

Figure 1: Impact of cadmium exposure to *C. reinardtii* grown in TAP_{EDDHA} medium. (A) Relative growth rate was expressed as the ratio µ/µ0 determined during the exponential phase

of growth after addition of 0, 10, 20, 30, 40, 50 and 70 µM of $CdCl_2$. (n=3 ± sd). µ = growth rate during cadmium exposure, μ_O = growth rate in control conditions. Black curve represents the dose-response effect calculated with the Hill model. Impact of a 70 µM Cd exposure on growth (B) and on chlorophyll concentration (C), and starch concentration (D) after a 48 h exposure. Significant differences with respect to the control condition at a significance level of 0.05 ($p<0.05$) are indicated by an asterisk (*).

Figure 2: Structure and elemental composition of *C. reinhardtii* cells exposed to cadmium. (A) Electron micrographs of two *C. reinhardtii* cells in control condition and (B) of two cells exposed to 70 µM Cd for 48 h , scale bar = 1 µm. Abbreviations: N, nucleus; P, pyrenoid; S, starch; Th, thylakoid; CW, cell wall. (C to H) Correlative TEM/X-EDS and NanoSIMS imaging of two cadmium exposed *C. reinhardtii* cells: (C and F) Electron micrographs of *C. reinhardtii* cells exposed to 70 µM Cd for 48 h, white arrows show the area analyzed by X-EDS analysis, scale bar = 1 µm. Abbreviations: N, nucleus; P, pyrenoid; S, starch; Th, thylakoid; V, vacuole; CV, contractile vacuole; CW, cellwall. (E and H) Corresponding NanoSIMS elemental maps obtained by Cs^+ ion source ($^{12}C^{14}N^-$ for N detection, $^{32}S^-$) and O^- RF plasma ion source ($^{31}P^+$, $^{40}Ca^+$), 10×10 µm² (E) and 12×12 µm² (H) fields of 256×256 pixels, scale bar = 2 µm. (D and G) X-EDS spectra of vacuoles and pyrenoid located on electron micrographs, copper signal is produced by the copper grid

Figure 3: In situ cadmium localization and speciation in *C. reinhardtii* exposed to 70 µM Cd for 48 in TAP_{EDDHA} medium. (A) False color µ-XRF elemental maps of Cd, S, P and Ca, arrows show points of interest where µ-XANES analyses were performed, scale bar = 2 µm. Step size = 0.4 µm, dwell-time = 300 ms/pixel at 3570 eV for S, P, Cd and at 4100 eV for Ca. (B) Two or three components fits (dotted line) of Cd L_{III}-edge µ-XANES spectra (solid line) of points of interest marked by arrows and of bulk sample; (C) Derivative of Cd L_{III}-edge µXANES; (D)

Distribution of Cd ligands after normalization of the percentages to 100%. The uncertainty is estimated to ±10%.

Figure 4: Carbon assimilation in *C. reinhardtii* grown in TAP_{EDDHA} medium (labeled ^{13}C-[1,2] acetate). (A and B) $^{13}C/^{12}C$ isotope ratio images obtained by NanoSIMS using Cs^+ source. The analyzed fields of 256×256 pixels were, from left to right, 12×12 µm², 8×8 µm², 10×10 µm² for control conditions (A) and 12×12 µm², 10×10 µm², 10×10 µm² for cadmium exposure conditions (70 µM Cd for 48 h) (B), scale bar = 2 µm, ROI and annotations for pyrenoid and starch plates are shown in Figure S1. (C) Impact of 70 µM Cd exposure for 48 h on ^{13}C isotopic enrichment in the pyrenoid and in starch plates (n=6 ± sd). Isotopic distribution of carbon in starch plates obtained from $f_{acetate}$ and f_{CO2} (D) and in starch carbon equivalent (E), (n =6 ± sd). Significant differences with respect to the control condition according to Kruskal-Wallis one-way analysis of variance on ranks ($p<0.05$) are indicated by an asterisk (*).

Figure 5: Proposed model of cadmium impact on the assimilation of carbon in *Chlamydomonas reinhardtii* in mixotrophic conditions. The description of the general metabolic pathways for carbon assimilation from organic (acetate) and inorganic (CO_2) sources are adapted from Johnson & Alric (2013). Under exposure conditions, cadmium is highly sequestered in the pyrenoid by sulfur ligands, impairing the Calvin cycle. Thus, CO_2 and acetate assimilation involving the Calvin cycle is limited (thin grey arrows) whereas acetate assimilation through glyoxylate cycle is favored (thick blue arrows). In addition, the anaplerotic PEPC activity could hypothetically participate in inorganic carbon fixation. Starch is accumulated in the chloroplast to prevent cellular troubles due to Cd stress. Finally, Cd is also sequestered in vacuoles, coordinated by phosphate ligands. Abbreviations: *SDH*, Succinate dehydrogenase; *FUM*, Fumarase; *MDH*, Malate Dehydrogenase; *PCK*,

Phosphoenolpyruvate Carboxykinase; *PEPC*, Phosphoenolpyruvate carboxylase; *CAH*, Carbonic anhydrase.

SUPPORTING INFORMATION

Supporting information is available at the publisher's web-site. Supporting information is given to the composition of the TAP_{EDDHA} medium (**Table S1**), to the definition of regions of interest (ROI) in NanoSIMS $^{13}C/^{12}C$ images for data analysis (**Figure S1**), and to linear combination fits (LCFs) of XANES spectra (**Figure S2**).

Figure 1

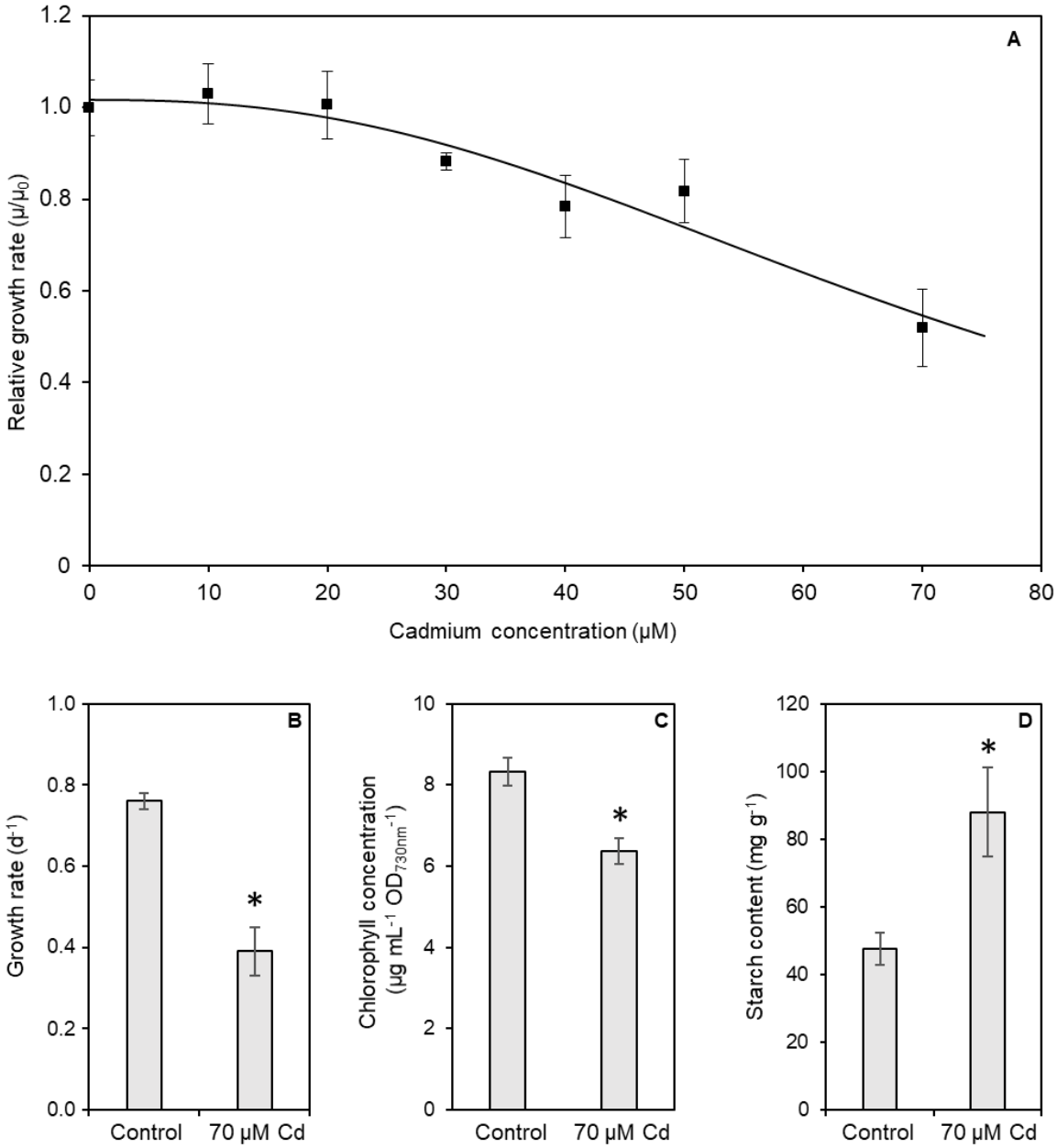

1071

1072

1073

1074

1075

1076

Figure 2

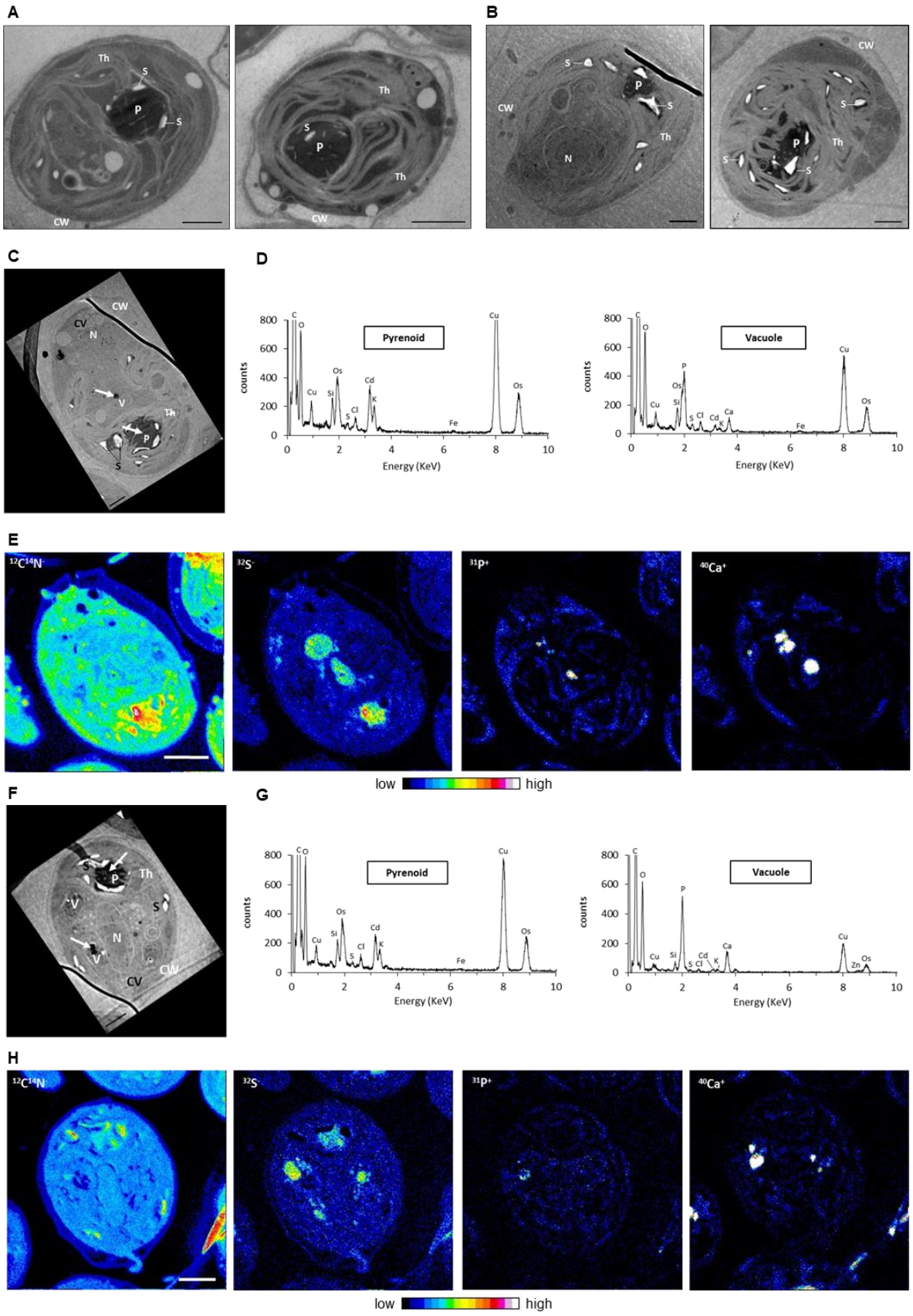
A
B
C
D
E
F
G
H
Th
S
P
CW
N
CV
V
Pyrenoid
Vacuole
counts
Energy (KeV)
low
high
12C14N-
32S-
31P+
40Ca+

Figure 3

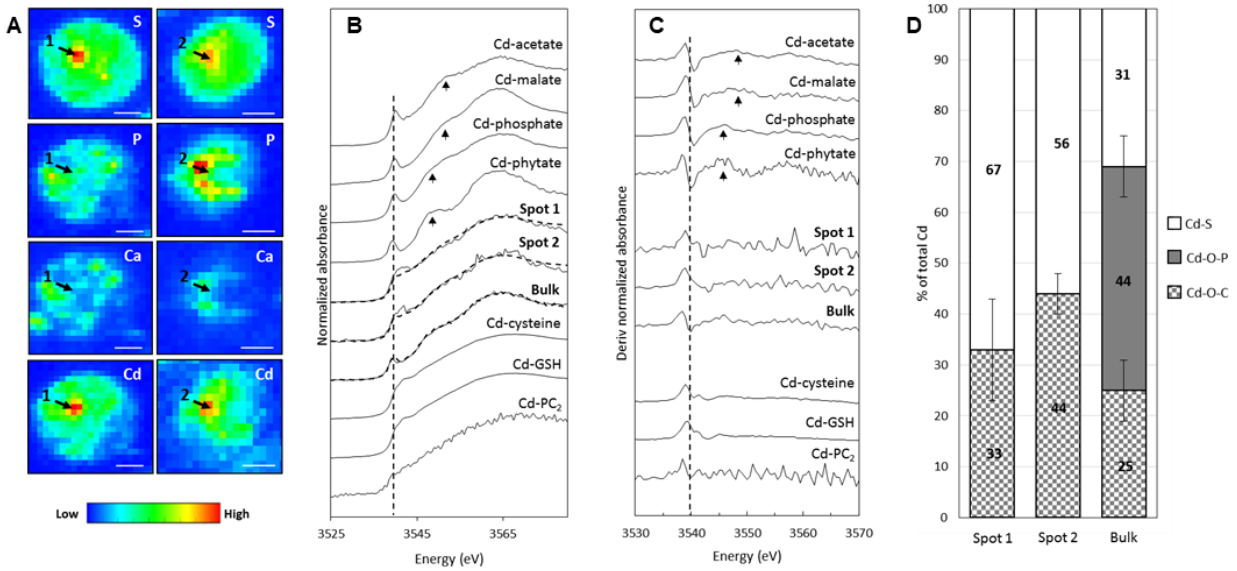

1102

1103

Figure 4

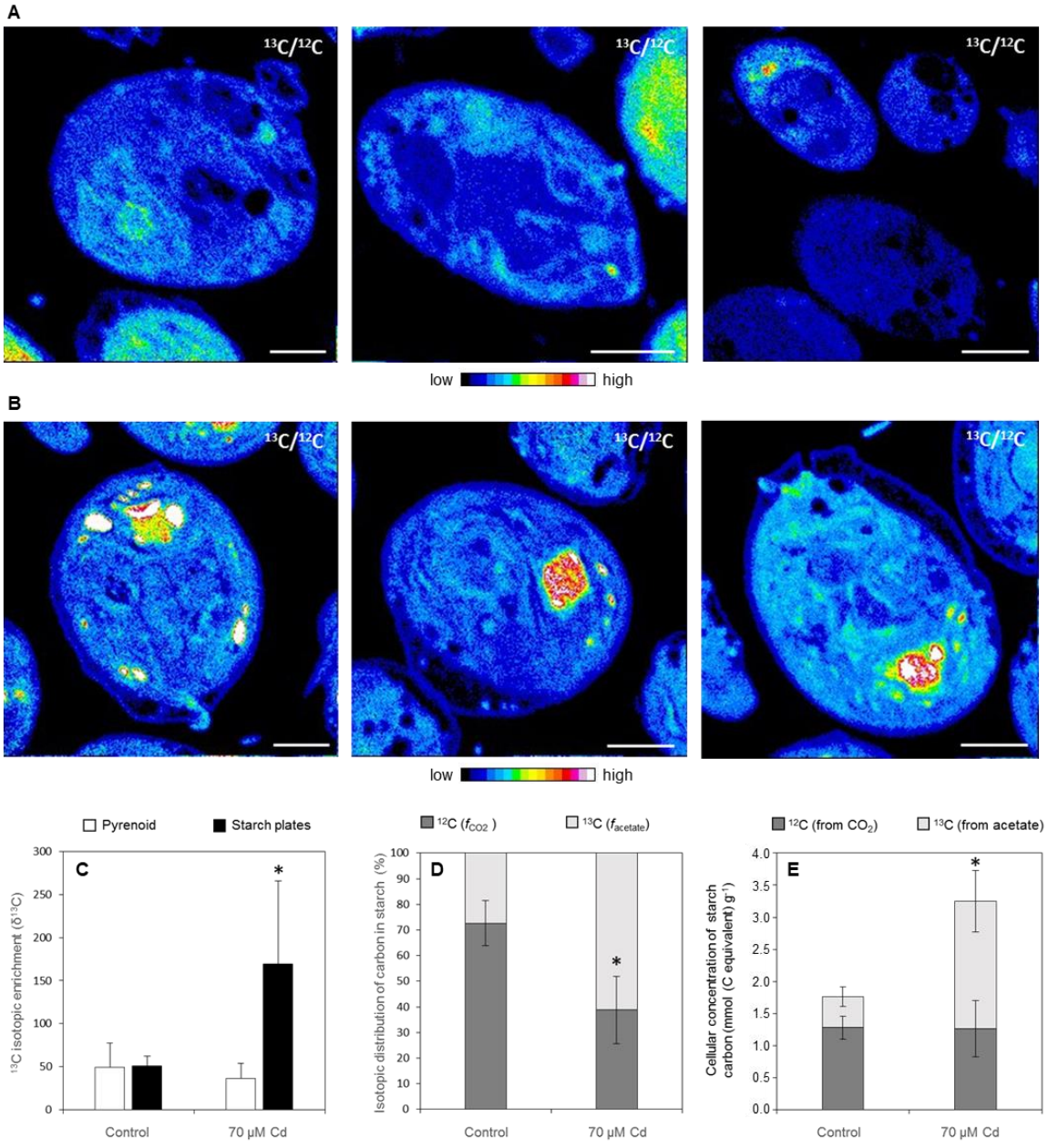
A
$^{13}C/^{12}C$
low
high
B
$^{13}C/^{12}C$
low
high
Pyrenoid
Starch plates
C
^{13}C isotopic enrichment ($\delta^{13}C$)
Control
70 µM Cd
^{12}C (f_{CO2})
^{13}C ($f_{acetate}$)
D
Isotopic distribution of carbon in starch (%)
Control
70 µM Cd
^{12}C (from CO_2)
^{13}C (from acetate)
E
Cellular concentration of starch carbon (mmol (C equivalent) g^{-1})
Control
70 µM Cd

Figure 5

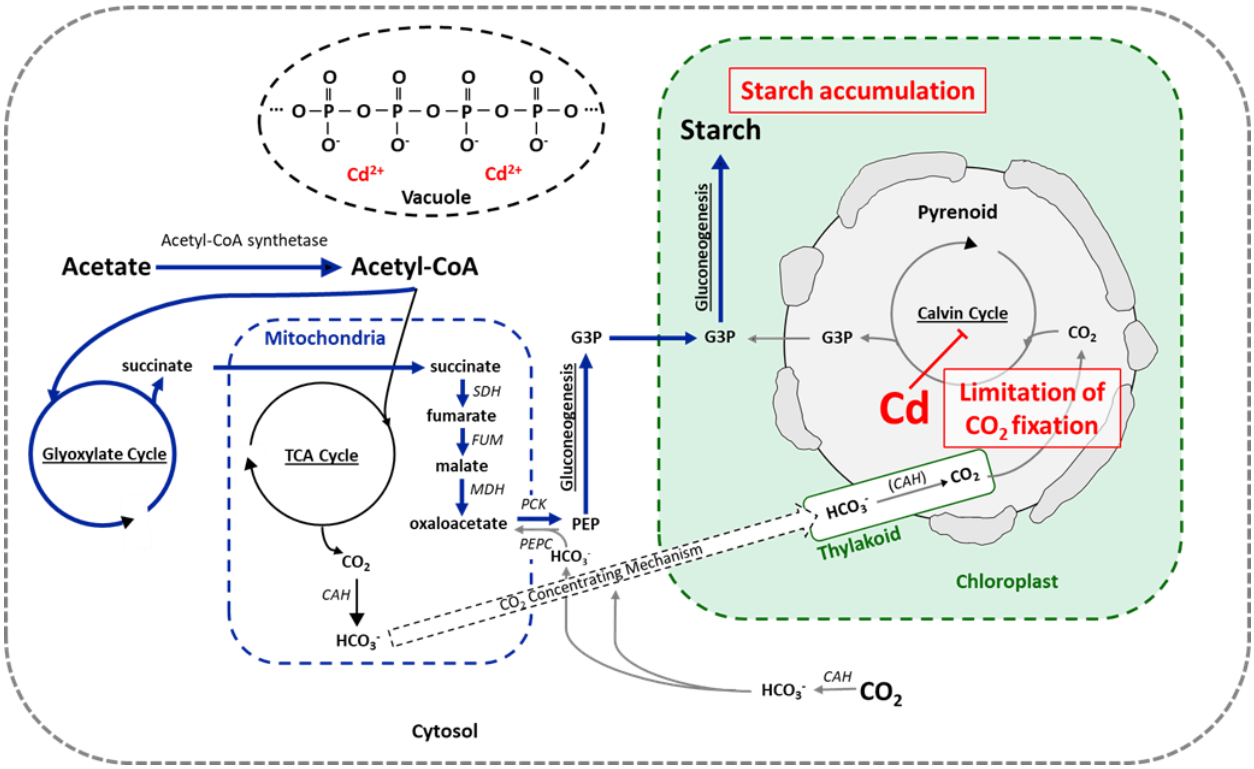

1111